TABLE 2
Tumor Glucose Metabolic Markers According to Uptake of ^{18}F-FDG and Index of GLUT-1 Positivity

Parameter	Control	Gemcitabine	Cyclophosphamide
Tumor uptake (%ID/g) × kg	0.743 ± 0.084	0.483 ± 0.118*	0.583 ± 0.142*
Blood uptake (%ID/g) × kg	0.048 ± 0.005	0.045 ± 0.011*	0.036 ± 0.007*
Muscle uptake (%ID/g) × kg	0.022 ± 0.002	0.021 ± 0.004*	0.026 ± 0.006*
T/B ratio	15.21 ± 1.487	9.885 ± 4.592*	12.21 ± 7.145*
T/M ratio	33.44 ± 4.721	15.15 ± 6.062*	7.859 ± 4.464*
GLUT-1 (intensity × %)	60.5 ± 5.6	58.3 ± 4.9	61.1 ± 6.9

*$P < 0.01$ compared with control group.
Data are mean ± SD.

12.29, and 117.3 ± 5.283 mg/dL and those at BS2 were 93.86 ± 13.45, 94.14 ± 14.70, and 91.86 ± 14.86 mg/dL in the gemcitabine-treated, cyclophosphamide-treated, and control groups, respectively. Both tumor weight and blood glucose level in all groups did not change significantly after chemotherapeutic treatment with gemcitabine and cyclophosphamide (Table 3).

DISCUSSION

This study demonstrated that tumor glucose utilization declined after a single dose of gemcitabine or cyclophosphamide, which was not based on reduced GLUT-1 expression. This decline in glucose utilization occurred at a time of increased apoptosis. These molecular events occurred before the actual tumor regression. These data suggest that apoptosis induced by chemotherapy is not always accompanied by glucose hypermetabolism for survival reactions as previously reported (*17,23*).

In clinical oncology, the decrease in ^{18}F-FDG uptake was usually associated with a good lesion response, especially in malignant lymphoma, esophageal cancer, and head and neck cancer (*13,14*). Recently, there have been reports that

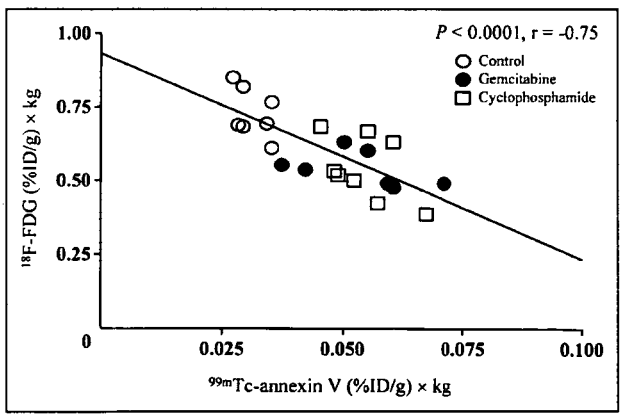

FIGURE 2. Negative correlation between ^{18}F-FDG uptake and ^{99m}Tc-annexin V uptake in control, gemcitabine-treated, and cyclophosphamide-treated groups. ^{18}F-FDG uptake ((%ID/g) × kg) = 0.932 − (6.956 ^{99m}Tc-annexin V uptake ((%ID/g) × kg)) ($r = -0.75$; $P < 0.01$).

^{99m}Tc-annexin V is very useful for detecting and in vivo imaging of apoptosis (*4,24,25*). The present study demonstrated that induction of apoptosis with a single dose of chemotherapy was associated with a striking reduction in ^{18}F-FDG uptake and a modest increase in annexin localization. Although appropriate chemotherapy induces metabolic regression (reflected by a reduction in ^{18}F-FDG uptake) before morphologic change of cancer tissue, the basic mechanism underlying the decrease in glucose uptake is not well understood. We observed that the uptake of ^{18}F-FDG was definitely decreased to approximately 55% of the control value by both gemcitabine and cyclophosphamide before the actual tumor regression. Both gemcitabine and cyclophosphamide themselves rarely affected blood glucose level, and our present results confirmed this observation. Mazurek et al. (*26,27*) suggested the following mechanisms: Chemotherapeutic agents damage DNA and then they activate adenosine diphosphate ribosyl transferase to repair DNA for proliferation. Because this repair requires a great amount of energy, intracellular nicotinamide adenine dinucleotide, which is an electron carrier, and adenosine triphosphate, which is required in intracellular phosphorylation, are so exhausted by anaerobic hyperglycolysis, they cannot compensate. This intracellular "famine" may depress important glycolytic enzymes. Consequently, glucose uptake in cancer cells decreases as a result of these intracellular reactions.

The relationship between apoptosis and glucose utilization at the early stage of cancer chemotherapy is also controversial (*17,28*). Haberkorn et al. reported an increase in glucose (^{18}F-FDG) uptake early after chemotherapy using gemcitabine for Morris hepatoma and interpreted it as a stress reaction of cancer cells as a protective mechanism against apoptosis (*17*). This interpretation may be reasonable since a great amount of energy is required for DNA repair. Furthermore, DNA damage promotes apoptosis via other pathways, such as the activation of tumor-suppression gene (e.g., p53) and inhibition of antiapoptotic molecules (e.g., Fas and phosphatidylinositol 3-phosphate kinase (PI3K-Akt)) (*29–32*). Activated caspases also have an essential role in the series of apoptosis. As a result of these

TABLE 3
Blood Glucose Level and Weight of Whole Body and Tumor

Parameter	Control	Gemcitabine	Cyclophosphamide	*P*
BS1 (mg/dL)	117.3 ± 5.283	114.1 ± 13.01	118.9 ± 12.29	ns
BS2 (mg/dL)	91.86 ± 14.86	93.86 ± 13.45	94.14 ± 14.70	ns
Whole-body weight (g)	209.6 ± 14.59	215.4 ± 14.29	204.9 ± 14.86	ns
Tumor weight (g)	3.503 ± 1.145	3.239 ± 1.520	4.168 ± 2.007	ns

ns = not significant.
Data are mean ± SD.

molecular interactions, an irreversible DNA-laddering reaction occurs at the end of programmed cell death. Because this reaction must use energy, glucose demand may increase temporarily. Occasionally, a "metabolic flare" was often observed on ^{18}F-FDG PET images after hormonal therapy was administrated for estrogen receptor–positive human breast cancer. This phenomenon may indicate responsiveness (*33*). Here, we speculated that tumor glucose hypometabolism was finally superior to the energy demand. Previous studies demonstrated maximal apoptosis 1 or 2 d after chemotherapy (*7,10,34*). Although ATP depletion and decrease in glucose uptake occur as apoptosis progresses after chemotherapy, these 2 phenomena themselves were reported to promote apoptosis (*26,35*). Thus, we confidently assumed that tumor glucose utilization after chemotherapy increasingly becomes hypometabolic and, finally, irreversible. Additionally, Spaepen et al. suggested that FDG uptake mainly correlates with the viable tumor cell fraction for 15-d monitoring of tumor response using a leukemia model in mice with severe combined immunodeficiency (*36*). However, changes in glucose metabolism by chemotherapy still remain to be clarified. Correlation between tumor uptake of ^{18}F-FDG and ^{99m}Tc-annexin V may help clarify the significance of early glucose utilization changes in clinical oncology. A long-time course of chemotherapeutic effects should also be evaluated in vivo models. Cremerius et al. reported FDG PET must be performed 2 wk after completion of therapy of metastatic germ cell tumor (*37*). Until the various histologic changes that influence glucose utilization become inactive, a high accuracy of FDG PET evaluation cannot be maintained. The serial ^{18}F-FDG and ^{99m}Tc-annexin V images each provide useful data for predicting a therapeutic response.

In this study, we investigated whether GLUT-1 expression affects tumor glucose utilization. However, GLUT-1 protein expression level did not change significantly after chemotherapy in our immunohistologic analyses. Histologic GLUT-1 overexpression correlated significantly with tumor characterization and prognosis in many cancer tissues. If ^{18}F-FDG uptake is high, GLUT-1 expression level also tends to be high. These findings are usually seen more with malignant lesions (*38*). In the present study, GLUT-1 expression was evaluated with "percent positive" and "intensity" per randomly selected high-power microscopic field. However, changes in cellularity by chemotherapy may affect the values of GLUT-1 expression rate if it is normalized to the cell number. Further evaluation considering the cellularity is needed to confirm the present results, although no apparent difference in the cell numbers (approximately 1,000 cells per field) was observed among the 3 groups. Unfortunately, little was known in our study as to why GLUT-1 positivity was not seemingly altered by chemotherapy. Using MR spectroscopy and western blotting, Rivenzon-Segal et al. suggested that glycolysis and GLUT-1 expression in breast tumor cells were positively correlated at both estrogen stimulation and tamoxifen inhibition (*39*). We deduce 2 points: (a) GLUT-1 protein expression is maintained for self-survival and (b) there is a time lag between the present protein expression on the cell surface and messenger RNA expression. Furthermore, this mechanism is more complicated because of the participation in hexokinase or the other GLUTs. Cyclophosphamide treatment was reported to modify tumor glycolytic rate and increase the intracellular lactate concentration in RIF-1 tumor (*40*).

In the present study, the animals were anesthetized with pentobarbital, which is known to depress glucose metabolism. This kind of barbiturate is a sedative-hypnotic drug, and its high lipophilicity has a direct effect on the central nervous system. The depressed glucose metabolism by pentobarbital may cause systemic errors. On the other hand, direct competition between FDG and blood glucose is regarded as the cause of impaired FDG uptake in tumors. Accordingly, we used anesthetized animals to avoid any physiologic variations, including blood glucose concentration, among the groups. It is also well known that blood glucose concentration is easily affected by any stress in awake animals.

The weakness of our study is the acute or chronic nature of our measurements. The animals received a single, high dose of chemotherapy to treat a rapidly growing tumor. The tumor response was evaluated within hours of chemotherapy administration. Whether serial administration of more moderate doses could produce a similar early result cannot be determined from the present study. However, there are clinical instances when an early indication of therapeutic

response is required. This is particularly necessary when toxic chemotherapy is used in tumors, such as gastric or lung cancer, where the response rate is around 50%. In those cases, an indication of nonresponse would permit a rapid redirection of therapy to other agents.

CONCLUSION

We found that the enhanced apoptotic reaction correlated with suppressed tumor glucose utilization after cytotoxic chemotherapy. The imaging results were confirmed by histologic evaluation. The decrease in tumor glucose utilization was independent of GLUT-1 overexpression. The increase in ^{99m}Tc-annexin V uptake in tumor as well as the decrease in ^{18}F-FDG uptake can be useful markers for predicting therapeutic outcomes and for prognosis at the early stage of chemotherapy.

ACKNOWLEDGMENTS

The authors are grateful to Professors Shinzo Nishi, Kazuo Miyasaka, and Koh-ichi Seki of the Central Institute of Isotope Science, Hokkaido University, for supporting this work. The authors also thank Koutaro Suzuki, Hidenori Katsuura, Hidehiko Omote, Hiroshi Arai, Keiichi Magota, and Miho Nakajima of the Facility of Radiology, Hokkaido University Medical Hospital, for assistance; Theseus Imaging Corp. for providing annexin V protein; and Makoto Sato, Sumitomo Heavy Industries, Ltd., for ^{18}F-FDG syntheses.

REFERENCES

1. Kerr JF, Wyllie AH, Currie AR. Apoptosis: a basic biological phenomenon with wide-ranging implications in tissue kinetics. *Br J Cancer.* 1972;26:239–257.
2. Thompson CB. Apoptosis in the pathogenesis and treatment of disease. *Science.* 1995;267:1456–1462.
3. Joseph B, Lewensohn R, Zhivotovsky B. Role of apoptosis in the response of lung carcinomas to anti-cancer treatment. *Ann NY Acad Sci.* 2000;926:204–216.
4. Belhocine T, Steinmetz N, Green A, Rigo P. In vivo imaging of chemotherapy-induced apoptosis in human cancers. *Ann NY Acad Sci.* 2003;1010:525–529.
5. Vermeersch H, Ham H, Rottey S, et al. Intraobserver, interobserver, and day-to-day reproducibility of quantitative ^{99m}Tc-HYNIC annexin-V imaging in head and neck carcinoma. *Cancer Biother Radiopharm.* 2004;19:205–210.
6. Ng SSW, Tsao MS, Chow S, Hedley DW. Inhibition of phosphatidylinositide 3-kinase enhances gemcitabine-induced apoptosis in human pancreatic cancer cells. *Cancer Res.* 2000;60:5451–5455.
7. Mochizuki T, Kuge Y, Zhao S, et al. Detection of apoptotic tumor response in vivo after a single dose of chemotherapy with ^{99m}Tc-annexin V. *J Nucl Med.* 2003;44:92–97.
8. Blankenberg FG, Katsikis PD, Tait JF, et al. In vivo detection and imaging of phosphatidylserine expression during programmed cell death. *Proc Natl Acad Sci USA.* 1998;95:6349–6354.
9. Kuge Y, Sato M, Zhao S, et al. Feasibility of ^{99m}Tc-annexin V for repetitive detection of apoptotic tumor response to chemotherapy: an experimental study using a rat tumor model. *J Nucl Med.* 2004;45:309–312.
10. Takei T, Kuge Y, Zhao S, et al. Time course of apoptotic tumor response following a single dose of chemotherapy: comparison with ^{99m}Tc-annexin V uptake and histologic findings in an experimental model. *J Nucl Med.* 2004;45:2083–2087.
11. Cohade C, Wahl RL. PET scanning and measuring the impact of treatment. *Cancer J.* 2002;8:119–134.
12. Rohren EM, Turkington TG, Coleman RE. Clinical applications of PET in oncology. *Radiology.* 2004;231:305–332.
13. Brun E, Kjellen E, Tennvall J, et al. FDG PET studies during treatment: prediction of therapy outcome in head and neck squamous cell carcinoma. *Head Neck.* 2002;24:127–135.
14. Spaepen K, Stroobants S, Verhoef G, Mortelmans L. Positron emission tomography with [^{18}F]FDG for therapy response monitoring in lymphoma patients. *Eur J Nucl Med Mol Imaging.* 2003;30(suppl 1):S97–S105.
15. Zhao S, Kuge Y, Tsukamoto E, et al. Effects of insulin and glucose loading on FDG uptake in experimental malignant tumours and inflammatory lesions. *Eur J Nucl Med.* 2001;28:730–735.
16. Mochizuki T, Tsukamoto E, Kuge Y, et al. FDG uptake and glucose transporter subtype expressions in experimental tumor and inflammation models. *J Nucl Med.* 2001;42:1551–1555.
17. Haberkorn U, Bellemann ME, Brix G, et al. Apoptosis and changes in glucose transport early after treatment of Morris hepatoma with gemcitabine. *Eur J Nucl Med.* 2001;28:418–425.
18. Wood BL, Gibson DF, Tait JF. Increased erythrocyte phosphatidylserine exposure in sickle cell disease: flow-cytometric measurement and clinical associations. *Blood.* 1996;88:1873–1880.
19. Tait JF, Smith C. Site-specific mutagenesis of annexin V: role of residues from Arg-200 to Lys-207 in phospholipid binding. *Arch Biochem Biophys.* 1991;288:141–144.
20. Tait JF, Engelhardt S, Smith C, Fujikawa K. Prourokinase-annexin V chimeras: construction, expression, and characterization of recombinant proteins. *J Biol Chem.* 1995;270:21594–21599.
21. Tait JF, Brown DS, Gibson DF, Blankenberg FG, Strauss HW. Development and characterization of annexin V mutants with endogenous chelation sites for ^{99m}Tc. *Bioconjug Chem.* 2000;11:918–925.
22. Zhao S, Kuge Y, Tsukamoto E, et al. Fluorodeoxyglucose uptake and glucose transporter expression in experimental inflammatory lesions and malignant tumours: effects of insulin and glucose loading. *Nucl Med Commun.* 2002;23:545–550.
23. Haberkorn U, Bellemann ME, Altmann A, et al. PET 2-fluoro-2-deoxyglucose uptake in rat prostate adenocarcinoma during chemotherapy with gemcitabine. *J Nucl Med.* 1997;38:1215–1221.
24. Belhocine T, Steinmetz N, Hustinx R, et al. Increased uptake of the apoptosis-imaging agent ^{99m}Tc recombinant human annexin V in human tumors after one course of chemotherapy as a predictor of tumor response and patient prognosis. *Clin Cancer Res.* 2002;8:2766–2774.
25. van de Wiele C, Lahorte C, Vermeersch H, et al. Quantitative tumor apoptosis imaging using technetium-99m-HYNIC annexin V single photon emission computed tomography. *J Clin Oncol.* 2003;21:3483–3487.
26. Mazurek S, Boschek CB, Eigenbrodt E. The role of phosphometabolites in cell proliferation, energy metabolism, and tumor therapy. *J Bioenerg Biomembr.* 1997;29:315–330.
27. Mazurek S, Eigenbrodt E. The tumor metabolome. *Anticancer Res.* 2003;23:1149–1154.
28. Moley KH, Mueckler MM. Glucose transport and apoptosis. *Apoptosis.* 2000;5:99–105.
29. Fresno Vara JA, Casado E, de Castro J, et al. PI3K/Akt signalling pathway and cancer. *Cancer Treat Rev.* 2004;30:193–204.
30. Raff M. Cell suicide for beginners. *Nature.* 1998;396:119–122.
31. Thorburn A, Thorburn J, Frankel AE. Induction of apoptosis by tumor cell-targeted toxins. *Apoptosis.* 2004;9:19–25.
32. Sellers WR, Fisher DE. Apoptosis and cancer drug targeting. *J Clin Invest.* 1999;104:1655–1661.
33. Mortimer JE, Dehdashti F, Siegel BA, et al. Metabolic flare: indicator of hormone responsiveness in advanced breast cancer. *J Clin Oncol.* 2001;19:2797–2803.
34. Blankenberg FG, Naumovski L, Tait JF, Post AM, Strauss HW. Imaging cyclophosphamide-induced intramedullary apoptosis in rats using ^{99m}Tc-radiolabeled annexin V. *J Nucl Med.* 2001;42:309–316.
35. Bacurau RF, O'Toole CE, Newsholme P, Costa Rosa LF. Sub-lethal concentrations of activated complement increase rat lymphocyte glutamine utilization and oxidation while lethal concentrations cause death by a mechanism involving ATP depletion. *Cell Biochem Funct.* 2002;20:183–190.
36. Spaepen K, Stroobants S, Dupont P, et al. [^{18}F]FDG PET monitoring of tumour response to chemotherapy: does [^{18}F]FDG uptake correlate with the viable tumour cell fraction? *Eur J Nucl Med Mol Imaging.* 2003;30:682–688.
37. Cremerius U, Effert PJ, Adam G, et al. FDG PET for detection and therapy control of metastatic germ cell tumor. *J Nucl Med.* 1998;39:815–822.
38. Medina RA, Owen GI. Glucose transporters: expression, regulation and cancer. *Biol Res.* 2002;35:9–26.
39. Rivenzon-Segal D, Boldin-Adamsky S, Seger D, Seger R, Degani H. Glycolysis and glucose transporter 1 as markers of response to hormonal therapy in breast cancer. *Int J Cancer.* 2003;107:177–182.
40. Poptani H, Bansal N, Jenkins WT, et al. Cyclophosphamide treatment modifies tumor oxygenation and glycolytic rates of RIF-1 tumors: ^{13}C magnetic resonance spectroscopy, Eppendorf electrode, and redox scanning. *Cancer Res.* 2003;63:8813–8820.

Biologic Correlates of Intratumoral Heterogeneity in ^{18}F-FDG Distribution with Regional Expression of Glucose Transporters and Hexokinase-II in Experimental Tumor

Songji Zhao, MD[1,2]; Yuji Kuge, PhD[2]; Takafumi Mochizuki, MD[3]; Toshiyuki Takahashi, MD[4]; Kunihiro Nakada, MD[1]; Masayuki Sato, BS[1]; Toshiki Takei, MD[1]; and Nagara Tamaki, MD[1]

[1]Department of Nuclear Medicine, Graduate School of Medicine, Hokkaido University, Sapporo, Japan; [2]Department of Tracer Kinetics, Graduate School of Medicine, Hokkaido University, Sapporo, Japan; [3]Department of Radiology, Nikko Memorial Hospital, Muroran, Japan; and [4]Department of Pathology, Hokkaido Gastroenterology Hospital, Sapporo, Japan

The biologic mechanisms involved in the intratumoral heterogeneous distribution of ^{18}F-FDG have not been fully investigated. To clarify factors inducing heterogeneous ^{18}F-FDG distribution, we determined the intratumoral distribution of ^{18}F-FDG by autoradiography (ARG) and compared it with the regional expression levels of glucose transporters Glut-1 and Glut-3 and hexokinase-II (HK-II) in a rat model of malignant tumor. **Methods:** Rats were inoculated with allogenic hepatoma cells (KDH-8) into the left calf muscle (n = 7). Tumor tissues were excised 1 h after the intravenous injection of ^{18}F-FDG and sectioned to obtain 2 adjacent slices for ARG and histochemical studies. The regions of interest (ROIs) were placed on ARG images to cover mainly the central (CT) and peripheral (PT) regions of viable tumor tissues and necrotic/apoptotic (NA) regions. The radioactivity in each ROI was analyzed quantitatively using a computerized imaging analysis system. The expression levels of Glut-1, Glut-3, and HK-II were determined by immunostaining and semiquantitative evaluation. The hypoxia-inducible factor 1α (HIF-1α) was also immunostained. **Results:** ARG images showed that intratumoral ^{18}F-FDG distribution was heterogeneous. The accumulation of ^{18}F-FDG in the CT region was the highest, which was 1.6 and 2.3 times higher than those in the PT and NA regions, respectively ($P < 0.001$). The expression levels of Glut-1, Glut-3, and HK-II were markedly higher in the CT region ($P < 0.001$) compared with those in the PT region. The intratumoral distribution of ^{18}F-FDG significantly correlated with the expression levels of Glut-1, Glut-3, and HK-II ($r = 0.923$, $P < 0.001$ for Glut-1; $r = 0.829$, $P < 0.001$ for Glut-3; and $r = 0.764$, $P < 0.01$ for HK-II). The positive staining of HIF-1α was observed in the CT region. **Conclusion:** These results demonstrate that intratumoral ^{18}F-FDG distribution corresponds well to the expression levels of Glut-1, Glut-3, and HK-II. The elevated expression levels of Glut-1, Glut-3, and HK-II, induced by hypoxia (HIF-1α), may be contributing factors to the higher ^{18}F-FDG accumulation in the CT region.

Key Words: ^{18}F-FDG; glucose transporters; hexokinase; heterogeneity; tumor

J Nucl Med 2005; 46:675–682

PET using ^{18}F-FDG has been widely used not only for detecting and staging malignant tumors but also for monitoring therapy response and for differentiating malignant lesions from benign lesions (*1–4*). These applications are based on the increased ^{18}F-FDG uptake due to enhanced glucose utilization in most tumors. The increased ^{18}F-FDG accumulation in malignant tumors is associated with the rate of transport across the cell membrane, the activity of hexokinase, and the rate of dephosphorylation in the tissue (*5,6*). The transport of ^{18}F-FDG across cell membranes is mediated by ≥5 structurally related proteins (constituting a family of glucose transporters, Glut-1 to Glut-5) (*7,8*). Significantly elevated expression levels of Glut-1 and Glut-3 are considered to be a factor contributing to the accumulation of ^{18}F-FDG in malignant tumors (*9–13*). It has also been suggested that the activity level of hexokinase-II (HK-II) contributes to ^{18}F-FDG accumulation in various malignant tumors (*14*). These studies, however, used PET or tissue-counting techniques and correlated average ^{18}F-FDG accumulation in the tumor with protein expression.

It is well known that various components, including nonmalignant components, are involved in most solid tumors (*15–17*). Tumor tissues also show intratumoral heterogeneity in their various properties, which may originate from the diverse phenotypic properties of tumor cells or may be induced by their metabolic microenvironment (*18–20*). In this regard, intratumoral heterogeneity in ^{18}F-FDG distribution has been well demonstrated by autoradiography (ARG)

Received Sep. 3, 2004; revision accepted Nov. 23, 2004.
For correspondence or reprints contact: Nagara Tamaki, MD, Department of Nuclear Medicine, Graduate School of Medicine, Hokkaido University, Kita 15 Nishi 7, Kita-ku, Sapporo 060-8638, Japan.
E-mail: natamaki@med.hokudai.ac.jp

(*15*). However, there have been few reports regarding the biologic mechanisms involved in the intratumoral heterogeneous distribution of ^{18}F-FDG. The relationships between the intratumoral distribution of ^{18}F-FDG and the regional expression of glucose transporters or hexokinases remain to be investigated. Such data should be helpful in understanding the mechanism of ^{18}F-FDG uptake in malignant tumors and should provide the biologic basis for diagnosing, staging, and prognosticating malignant tumors and monitoring therapy response by ^{18}F-FDG PET.

To clarify factors inducing heterogeneous ^{18}F-FDG distribution, we determined in this study the intratumoral distribution of ^{18}F-FDG by ARG and compared it with the regional expression levels of Glut-1, Glut-3, and HK-II in a rat model of malignant tumor.

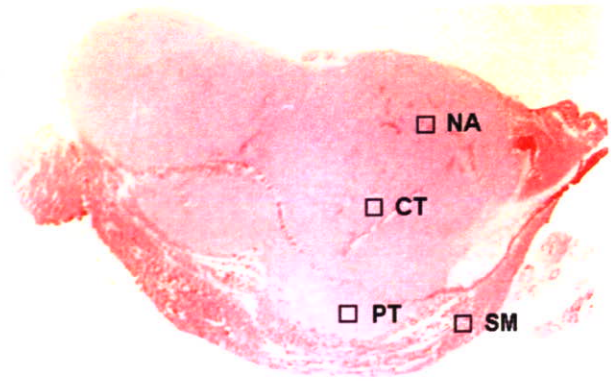

FIGURE 1. ROIs were placed on ARG image, to cover mainly central (CT) and peripheral (PT) regions of viable tumor tissues and necrotic/apoptotic (NA) regions, with reference to corresponding sections stained with HE. SM = surrounding muscle.

MATERIALS AND METHODS

Animal Studies

The experimental protocol was completely approved by the Laboratory Animal Care and Use Committee of Hokkaido University. Male Wistar King Aptekman/hok (WKAH) rats, weighing 203–268 g, were inoculated with a suspension of allogenic hepatoma cells (KDH-8, 1×10^6 cells per rat) into the left calf muscle. Two weeks after the tumor inoculation, when the tumors were 2–3 cm in diameter, the rats were fasted overnight ($n = 7$) (*21*). Each rat was anesthetized with pentobarbital (50 mg/kg body weight, intraperitoneally) and was injected in the tail vein with 37 MBq of ^{18}F-FDG synthesized as previously described (*22*). Sixty minutes after the ^{18}F-FDG injection, the animals were sacrificed and the tumors were quickly excised. Each tumor tissue was then sectioned at 2- to 3-mm thickness to obtain 2 adjacent slices. One of the 2 slices was embedded in Tissue-Tek medium (Sakura Finetechnical Co., Ltd.) and frozen in isopentane/dry ice for ARG studies. Formalin-fixed, paraffin-embedded specimens were prepared using the other slice for subsequent histochemical studies (*23*).

ARG Studies

The frozen samples were cut into 20-μm sections with a CM3050-Cryostat (Leica) at −20°C. The tumor sections were placed in a phosphor image plate cassette, together with a set of calibrated standards (*17*), and an overnight ARG exposure was used to detect the distribution of ^{18}F-FDG. The tumor sections (10 μm) adjacent to those used for the ARG studies were stained with hematoxylin and eosin (HE) for use as the reference to determine the regions of interest (ROIs) on the autoradiograms.

The ARG images were analyzed using a computerized imaging analysis system (BAS 5000 Bio-Imaging Analyzer; Fuji Photo Film Co., Ltd.). The resolution of ARG of the BAS 5000 is 100 μm. To quantitatively evaluate the distribution of ^{18}F-FDG radioactivity, 32 ROIs (0.36 mm^2) were determined on each ARG image. ROIs were placed to cover mainly the central (CT; $n = 8$) and peripheral (PT; $n = 8$) regions of the viable tumor tissues, necrotic/apoptotic (NA; $n = 8$) regions, and the surrounding muscle (SM; $n = 8$), by referring to the sections stained with HE (Fig. 1); each ROI was selected microscopically by a pathologist and identified by its predominant histologic characteristic as a region of the viable tumor cells and necrotic/apoptotic cells in the CT and PT regions on the HE section. Large necrotic regions occasionally observed in the center of the tumors were excluded from the evaluation. To avoid any bias, these ROIs were determined in a blind manner for ARG images and immunologic staining (Gluts and HK-II). The ROIs placed on HE images were transferred to ARG images by using computer software (MCID-M2 Image Analyzer; Imaging Research Inc.). Briefly, coordinates were set on both HE and ARG images, the coordinates of each ROI on the HE images was determined, and then each ROI was transferred to the same coordinates of the corresponding ARG images. The radioactivity in each ROI was shown by photostimulated luminescence per unit area, PSL/mm^2 (PSL = a·D·t: a = constant; D = radioactivity exposed on imaging plate; t = exposed time); then each count of PSL/mm^2 from a tumor section was recorded and used to calculate the mean counts per mm^2 and converted to the percentage injected dose per gram (%ID/g) of tissue by using activity of the standards, with the assumption that tissue density is 1 g/cm^3 (*17,24*). The mean radioactivities of the 8 ROIs determined for the CT, PT, NA regions, and SM, respectively, were used to evaluate the ^{18}F-FDG accumulation in the tissues.

Histochemical Studies

The expression of Glut-1, Glut-3, and HK-II was studied in the sections of a formalin-fixed, paraffin-embedded tumor according to a standard immunostaining procedure (*10,25*). Briefly, after deparaffization and rehydration, endogenous peroxidase activity was blocked for 10 min in methanol containing 3% hydrogen peroxide. Thereafter, endogenous nonspecific antigens were blocked in 10% normal goat albumin (HISTOFINE SAB-PO kit; Nichirei) for 10 min at 37°C and then incubated with an anti-Glut-1, anti-Glut-3, or antihexokinase II antibody (Chemicon International Inc.) for 30 min at 37°C. The bound antibody was visualized using the avidin/biotin conjugate immunoperoxidase procedure (ABC) with the HISTOFINE SAB-PO kit and 3,3′-diaminobenzidine tetrahydrochloride. Tumor sections adjacent to those used for these histochemical studies were also stained with anti-HIF-1α (mouse antihypoxia-inducible factor 1α monoclonal IgG 2b, clone H1α67; Novus Biologicals) using the method of Zhong et al. (*26*) with slight modification. Briefly, after deparaffinization and rehydration, the slides were initially immersed in a target retrieval solution (10 mmol/L ethylenediaminetetraacetic acid, pH 8.0) and heated in a microwave oven (500 W) for 20 min.

After the antigen retrieval, endogenous peroxidase activity was blocked for 5 min in methanol containing 3% hydrogen peroxide. Thereafter, endogenous nonspecific antigens were blocked in 10% hog albumin (Cosmo Bio., Ltd.) for 10 min and then incubated overnight with the primary antibody at 4°C. Finally, the bound antibody was visualized using the ABC procedure with the HISTOFINE MAX-PO (M) kit (Nichirei) and 3,3′-diaminobenzidine tetrahydrochloride. Tumor sections adjacent to those used for the immunostaining were stained with HE.

For immunohistochemical grading, ROIs placed on the HE-stained sections were transferred to immunologically stained sections as described. The intensity of staining and the percentage of positively stained cells in the CT (n = 8) and PT (n = 8) regions of the viable tumor tissues were evaluated microscopically. The intensity of staining (intensity) was graded from 0 to 3 (0 = not stained, 1 = equivocal, 2 = intense, and 3 = very intense) according to the criteria of Higashi et al. (*27*). Moreover, the percentage of positively stained cells (% positive) was classified from 1 to 5 (1 = 0%–20%, 2 = 20%–40%, 3 = 40%–60%, 4 = 60%–80%, and 5 = 80%–100%). The expression levels of Gluts and HK-II were assessed semiquantitatively using the product of these scores (intensity × % positive) (*28*). In HIF-1α staining, cells with completely and darkly stained nuclei were regarded as positively stained cells (*29*).

Statistical Analysis

All values are expressed as mean ± SD. One-way ANOVA and the Bonferroni post hoc test were used to assess the significance of differences due to the intratumoral distribution of ^{18}F-FDG. To evaluate the significance of differences in the expression levels of Glut-1, Glut-3, and HK-II (intensity × % positive) between the CT and PT regions, an unpaired Student t test was performed. Simple regression analysis was used to compare the intratumoral ^{18}F-FDG distribution and the expression levels of Glut-1, Glut-3, and HK-II. A 2-tailed P value < 0.05 was considered significant.

RESULTS

Intratumoral Distribution of ^{18}F-FDG

Figure 2A shows the representative autoradiogram of ^{18}F-FDG distribution in the tumor. The ARG images showed heterogeneous ^{18}F-FDG distribution with a relatively higher ^{18}F-FDG accumulation level in the CT regions of viable tumor tissues.

Results from the quantitative evaluation of ^{18}F-FDG distribution are summarized in Figure 2B. The accumulation of ^{18}F-FDG in the CT region was the highest (4.43 ± 0.50 %ID/g), which was 1.6 and 2.3 times higher than those in the PT region (2.85 ± 0.22 %ID/g) and the NA region (1.94 ± 0.10 %ID/g), respectively ($P <$ 0.001). The accumulation of ^{18}F-FDG in the PT region was 1.5 times and was significantly higher than that in the NA region ($P < 0.001$). The distribution of ^{18}F-FDG in the SM (0.18 ± 0.01 %ID/g) was lower than those in any other ROIs determined in the tumor tissues (CT, PT, and NA).

Immunohistochemical Staining

The typical immunostaining of Glut-1, Glut-3, and HK-II in the CT and PT region is shown in Figure 3. The intensity and extent of staining of Glut-1, Glut-3, and HK-II were markedly higher in the CT region than those in the PT region.

The results of immunohistochemical grading are summarized in Figure 4. The histochemical grading scores for Glut-1 and Glut-3 were significantly higher in the CT region (11.34 ± 1.78 for Glut-1 and 6.02 ± 1.83 for Glut-3) than those in the PT region (4.23 ± 0.85 for Glut-1 and 2.29 ± 0.62 for Glut-3; $P < 0.001$ for both). The histochemical grading score for HK-II was also significantly higher in the

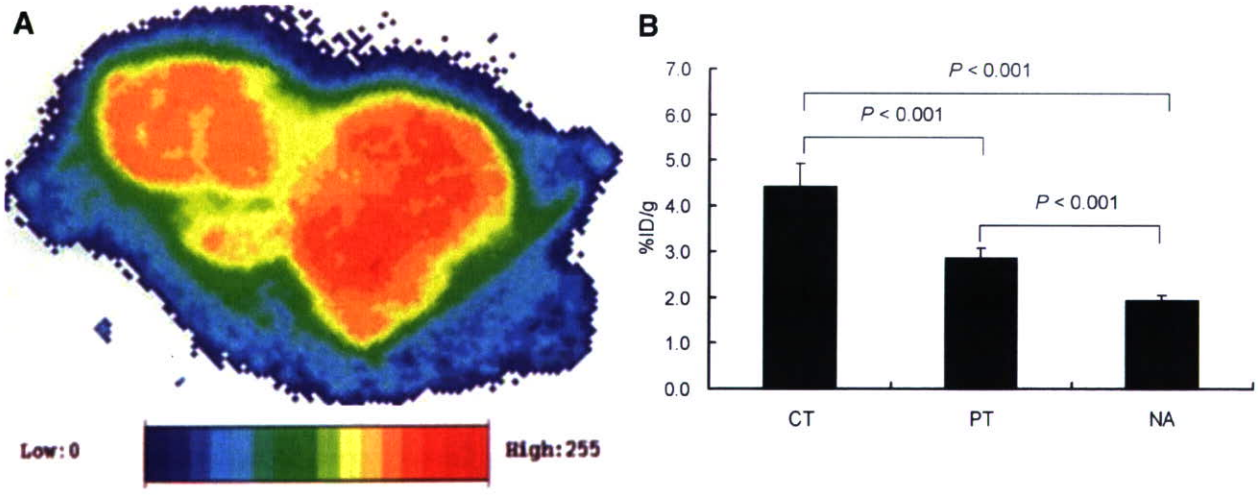

FIGURE 2. (A) Representative autoradiograph of ^{18}F-FDG distribution. ARG image shows intratumoral heterogeneous ^{18}F-FDG distribution. (B) Quantitative evaluation of intratumoral ^{18}F-FDG distribution. ^{18}F-FDG accumulation level in CT region was highest, which was 1.6 and 2.3 times higher than those in PT and NA regions, respectively ($P < 0.001$).

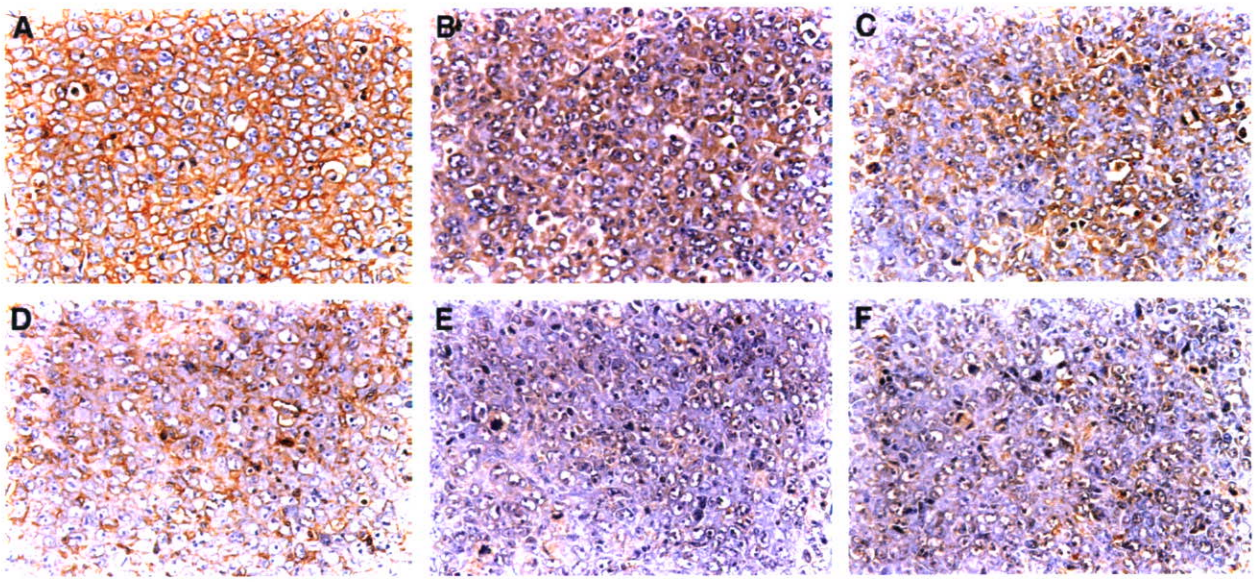

FIGURE 3. Staining with anti-Glut-1 (A and D), anti-Glut-3 (B and E), and anti-HK-II (C and F) antibodies in CT region (top) was more prominent than those in PT region (bottom) in KDH-8 tumor tissues, respectively (×400).

CT region (4.25 ± 0.98) compared with that in the PT region (2.00 ± 0.28; $P < 0.001$). The positive staining of HIF-1α was clearly observed in the CT region (Fig. 5) but not in the PT region.

Relationships Between ^{18}F-FDG Accumulation and Expression Levels of Gluts and HK-II

The accumulation of ^{18}F-FDG and the expression levels of Glut-1, Glut-3, and HK-II were significantly higher in the CT region than those in the PT region (Figs. 2 and 4). Figure 6 shows scattergrams of histochemical grading scores and ^{18}F-FDG accumulation. Intratumoral ^{18}F-FDG accumulation significantly correlated with the expression levels of Glut-1, Glut-3, and HK-II: $r = 0.923$, $P < 0.001$ for Glut-1; $r = 0.829$, $P < 0.001$ for Glut-3; and $r = 0.764$, $P < 0.01$ for HK-II.

DISCUSSION

In this study, a relatively higher ^{18}F-FDG accumulation was observed in the CT regions, with elevated expression levels of Glut-1, Glut-3, and HK-II. Positive staining of HIF-1α was observed in these regions. Intratumoral ^{18}F-FDG distribution significantly correlated with the expression levels of Glut-1, Glut-3, and HK-II. Consequently, the regional expression levels of Glut-1, Glut-3, and HK-II may increase in a hypoxic environment within tumor tissues and may contribute to heterogeneous ^{18}F-FDG distribution in the tumor tissues.

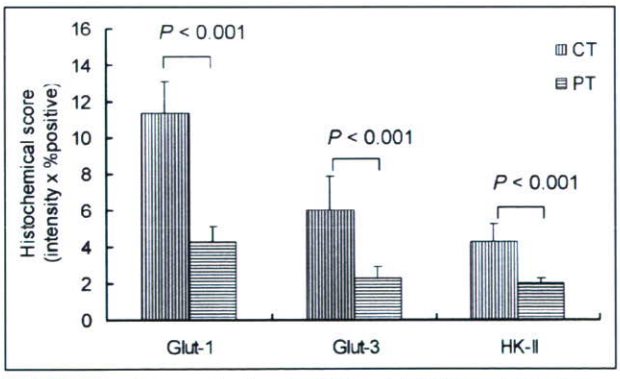

FIGURE 4. Expression levels of Glut-1, Glut-3, and HK-II were assessed by semiquantitative immunohistochemical grading performed by calculating the product of these scores (intensity × % positive). Histochemical scores of Glut-1, Glut-3, and HK-II were significantly higher in CT region than those in PT region ($P < 0.001$).

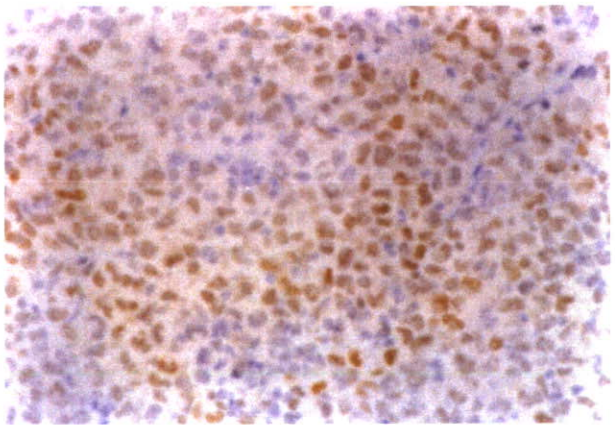

FIGURE 5. Positive staining of HIF-1α was clearly observed in CT region (×400).

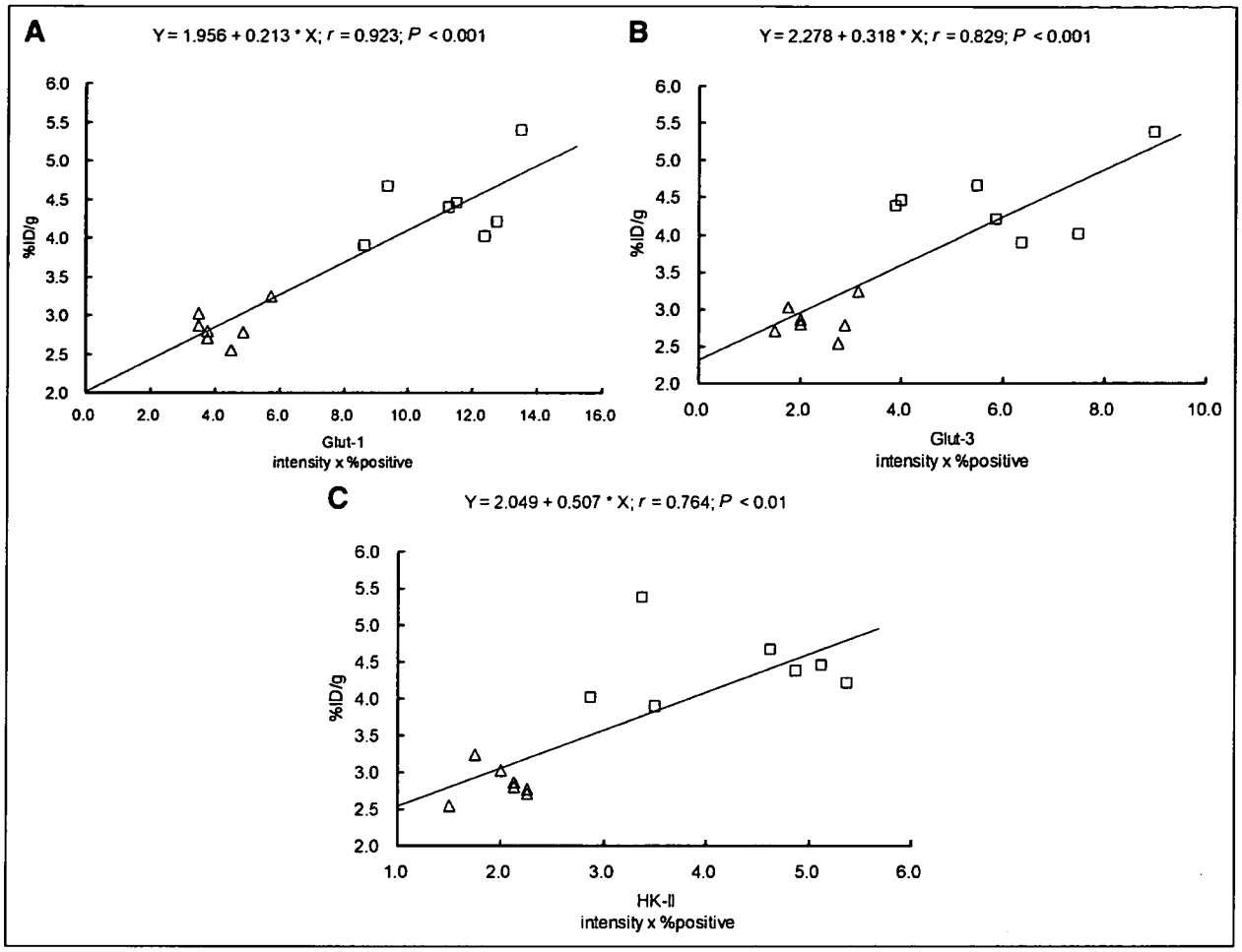

FIGURE 6. Relationships between expression levels of Glut-1, Glut-3, and HK-II and intratumoral ^{18}F-FDG accumulation in KDH-8 tumor tissues. Intratumoral ^{18}F-FDG accumulation significantly correlated with expression levels of Glut-1, Glut-3, and HK-II (intensity × % positive). (A) Relationship between ^{18}F-FDG accumulation and histochemical grading score for Glut-1. (B) Relationship between ^{18}F-FDG accumulation and histochemical grading score for Glut-3. (C) Relationship between ^{18}F-FDG accumulation and histochemical grading score for HK-II. □, CT region; △, PT region.

Although intratumoral heterogeneity in ^{18}F-FDG distribution has been demonstrated (*15*), there have been few reports with regard to the biologic mechanisms involved in the intratumoral heterogeneous distribution of ^{18}F-FDG. The present results showed a significant correlation between the intratumoral distribution of ^{18}F-FDG and the regional expression level of Glut-1, which is consistent with the results of syngeneic rat mammary cancer reported by Brown et al. (*30*). In addition, our results demonstrated—to our knowledge, for the first time—that intratumoral ^{18}F-FDG distribution significantly correlates with the regional expression levels of Glut-3 and HK-II. The heterogeneity in ^{18}F-FDG distribution may be ascribed to the altered expression levels of Glut-1, Glut-3, and HK-II and may reflect a metabolic microenvironment of tumors.

Aggressive tumors often have insufficient blood supply. Hypoxia occurs in tissue that is >100–200 μm away from a functional blood supply. When the tumors are exposed to a hypoxic environment, HIF-1α is activated to promote the transcription of several genes, including glucose transporters and glycolytic enzymes (*31*). The increased uptake of ^{3}H-FDG in vitro by hypoxic tumor cells has been well demonstrated (*32*). Recently, Dearling et al. (*33*) have extended the previous in vitro work and confirmed the selectivity of ^{18}F-FDG for hypoxic regions over normoxic regions in vivo. In the present study, a relatively higher ^{18}F-FDG accumulation was observed in the CT region, with elevated expression levels of Glut-1, Glut-3, and HK-II. The positive staining of HIF-1α was observed in these regions. Taken altogether, the regional expression levels of Glut-1, Glut-3, and HK-II may be increased by HIF-1α in a hypoxic environment within the tumor tissue and may contribute to the elevated ^{18}F-FDG accumulation.

Several studies have focused on the expression of Gluts and hexokinase activity to define the role of these proteins in the regulation of ^{18}F-FDG accumulation (*34,35*). Elevated expression levels of Glut-1 and Glut-3 are considered to be factors that contribute to the accumulation of ^{18}F-FDG in malignant tumors (*9–13,23,28*). It has also been suggested that the activity level of HK-II contributes to ^{18}F-FDG accumulation in various malignant tumors (*14*). Chromatographic, polyclonal antibody, and amino acid analyses indicated that rat hepatoma hexokinase is most closely related to HK-II and suggests that mitochondrial hexokinase activity determines the rate of accumulation of ^{18}F-FDG in tumors (*36*). These studies, however, used PET or tissue-counting techniques and correlated average ^{18}F-FDG accumulation in the tumor with protein expression. The biologic mechanisms involved in intratumoral heterogeneity in ^{18}F-FDG distribution have not been fully investigated. The present results demonstrate that the expression levels of Glut-1, Glut-3, and HK-II also contribute to intratumoral heterogeneity in ^{18}F-FDG distribution in our model rats, as determined using an ARG technique. It is crucial to consider the relative contributions of Glut-1, Glut-3, and HK-II to intratumoral ^{18}F-FDG accumulation. Unfortunately, we could not determine the relative contributions of these proteins, mainly due to the limited number of samples used in this study. Further studies are required to clarify the respective contributions of glucose transporters and hexokinase to intratumoral heterogeneity in ^{18}F-FDG accumulation.

Intratumoral ^{18}F-FDG distribution has been described at the cellular level by several investigators (*15–20*). Kubota et al. showed that ^{18}F-FDG preferentially accumulates in macrophages and young granulation tissues surrounding necrotic foci rather than in tumor cells using a malignant tumor mouse model (*15*). In contrast, Brown et al. (*17*) observed relatively less ^{3}H-FDG accumulation in necrotic/inflammatory infiltration compared with that in the tumor cells. Our results in rats confirmed intratumoral heterogeneity in ^{18}F-FDG distribution. The ^{18}F-FDG accumulation in the CT regions was 1.6 and 2.3 times higher than those in the PT and NA regions, respectively. Our results are consistent with the results reported by Brown et al.

In this study, the regions of viable tumor tissues and NA regions in ARG were identified using the HE-stained sections as reference. Apoptosis was most reliably assayed by morphologic counts using HE staining. Since there are some apoptotic cancer cells interwoven in necrotic regions and it was difficult to clearly distinguish apoptotic cells from necrotic cells in the present study, the term NA regions is used. Viable tumor cells and necrotic/apoptotic cells were also interwoven; thus, we used relatively small ROIs to clearly divide the regions between the viable tumor cells and necrotic/apoptotic cells. The larger ROIs appeared to cover both of the viable tumor cells and necrotic/apoptotic cells. Brown et al. (*17*) also used such ROI analysis to evaluate intratumoral distribution of ^{18}F-FDG. On the other hand, because necrotic cells revealed cell injuries in morphology—such as the cell membrane appearing ruptured, the nuclear chromatin being markedly condensed or pyknotic, vesicular structures filling the cytoplasm, and fusion of organelles (*37*)—the immunohistochemical staining of Glut-1, Glut-3, and HK-II cannot reflect the antigenicity of cells. Therefore, the expression levels of Glut-1, Glut-3, and HK-II were not investigated by immunostaining and semiquantitative evaluation in the NA regions. The slices immunohistochemically stained for Glut-1, Glut-3, and HK-II were from the formalin-fixed, paraffin-embedded specimens, but those used in ARG imaging to determine regional ^{18}F-FDG distribution were from the frozen samples. Thus, selected areas in the immunohistochemical staining for Glut-1, Glut-3, and HK-II of the CT, PT, and NA regions were not exactly congruent with those for determining regional ^{18}F-FDG distribution on ARG imaging, although both formalin-fixed, paraffin-embedded specimens and frozen samples were adjacent. It is important to note that expression of Glut-1, Glut-3, and hexokinase II (as determined in this study) does not generally imply increased functional activity. Several studies have demonstrated that hexokinase bound to the mitochondrial membrane has a much higher catalytic activity than cytosolic hexokinase. Aloj et al. (*14*) have also indicated that ^{18}F-FDG uptake correlates better with ^{18}F-FDG phosphorylating activity of mitochondrial preparations than with the level of expression of the Glut-1 or hexokinase I or II genes. The excellent correlation between HK-II expression and ^{18}F-FDG uptake observed in the present study may not be representative for other tumor models.

In our study, ARG imaging was performed 1 h after ^{18}F-FDG injection. The 1-h time point is widely used also in rodent models, and no significant differences in the ^{18}F-FDG uptake were observed in the mouse tumor tissues between 1 and 2 h after ^{18}F-FDG injection (*33*). However, further studies at more than one time point are needed to give an indication of the time course of ^{18}F-FDG uptake and to compare with the present results in rodent-bearing xenografts.

^{18}F-FDG PET has become increasingly important not only for detecting and staging malignant tumors but also for monitoring therapy response and for differentiating malignant lesions from benign lesions (*1–4*). However, variable tumor accumulation of ^{18}F-FDG has been indicated to prevent accurate diagnosis by ^{18}F-FDG PET (*38,39*). Intratumoral heterogeneity in ^{18}F-FDG distribution may also affect such diagnostic accuracy. The present study provides a biologic basis of intratumoral heterogeneity in ^{18}F-FDG distribution, which leads to better understanding of the mechanism of ^{18}F-FDG accumulation in tumors and contributes to the accurate diagnosis of patients with malignant tumors by ^{18}F-FDG PET. On the other hand, recent advances in radiation therapy such as intensity-modulated radiation therapy have exploited new areas for the use of

^{18}F-FDG PET (*40*). Regions of high ^{18}F-FDG uptake can be treated with a higher radiation dose compared with a hypometabolic portion of the same mass. In addition, glucose transporters (Glut-1 and Glut-3) and glycolytic enzymes (for example, hexokinase) are promoted by activated HIF-1α (*31*). The present study showed an excellent correlation between regional ^{18}F-FDG uptake and the expression of facilitative glucose transporters (Glut-1 and Glut-3) and HK-II. Furthermore, this study found that ^{18}F-FDG uptake was more intense in tumor regions that express HIF-1α. Recent clinical data indicate that hypoxic tumors are known to be more malignant, to be more likely to metastasize, and to have a poor prognosis. HIF-1α is considered to be a key factor for tumor progression by upregulating genes involved in angiogenesis, cell survival, cell invasion, and resistance to drug therapy and radiotherapy. Thus, the findings of this study suggest that tumor areas with high ^{18}F-FDG uptake may represent biologically more aggressive cancer cells. This has important consequences for the use of ^{18}F-FDG PET for treatment planning—particularly, intensity-modulated radiation therapy. ^{18}F-FDG PET could help to identify regions for dose-escalation protocols. We believe that our data also provide useful information in a precision radiation therapy protocol with modern radiotherapy modalities.

CONCLUSION

The colocalization of a high ^{18}F-FDG level and Glut-1, Glut-3, and HK-II overexpression in regions that are likely to be subjected to hypoxia as well as the strong correlation between the transporters and HK-II expression and ^{18}F-FDG accumulation suggest that enhanced transmembrane transport and phosphorylation may be part of an adaptive mechanism triggered by changes in the metabolic microenvironment of cancer cells. The regional expression levels of Glut-1, Glut-3, and HK-II may increase in a hypoxic environment within tumor tissues and may contribute to intratumoral heterogeneous ^{18}F-FDG distribution. The present results lead to a better understanding of the mechanism of ^{18}F-FDG accumulation in tumors, which may help in interpreting ^{18}F-FDG accumulation in patients with malignant tumors.

ACKNOWLEDGMENTS

This work was supported in part by a grant-in-aid for Scientific Research from the Japan Society for the Promotion of Science and in part by the Japanese Ministry of Education, Culture, Sports, Science and Technology and by a grant from the Rotary Yoneyama Memorial Foundation, Inc. The authors are grateful to the staff of the Nuclear Medicine and Central Institute of Isotope Science, Hokkaido University, for supporting this work. We also thank Mr. Kenichi Nishijima for technical assistance.

REFERENCES

1. Delbeke D, Rose DM, Chapman WC, et al. Optimal interpretation of FDG PET in the diagnosis, staging and management of pancreatic carcinoma. *J Nucl Med.* 1999;40:1784–1791.
2. Higashi T, Sakahara H, Torizuka T, et al. Evaluation of intraoperative radiation therapy for unresectable pancreatic cancer with FDG PET. *J Nucl Med.* 1999; 40:1424–1433.
3. Schelling M, Avril N, Nahrig J, et al. Positron emission tomography using [^{18}F]fluorodeoxyglucose for monitoring primary chemotherapy in breast cancer. *J Clin Oncol.* 2000;18:1689–1695.
4. Dimitrakopoulou-Strauss A, Strauss LG, Heichel T, et al. The role of quantitative ^{18}F-FDG PET studies for the differentiation of malignant and benign bone lesions. *J Nucl Med.* 2002;43:510–518.
5. Haberkorn U, Ziegler SI, Oberdorfer F, et al. FDG uptake, tumor proliferation and expression of glycolysis associated genes in animal tumor models. *Nucl Med Biol.* 1994;21:827–834.
6. Golshani-Hebroni SG, Bessman SP. Hexokinase binding to mitochondria: a basis for proliferative energy metabolism. *J Bioenerg Biomembr.* 1997;29:331–338.
7. Bell GI, Burant CF, Takeda J, Gould GW. Structure and function of mammalian facilitative sugar transporters. *J Biol Chem.* 1993;268:19161–19164.
8. Brown RS, Leung JY, Kison PV, Zasadny KR, Flint A, Wahl RL. Glucose transporters and FDG uptake in untreated primary human non-small cell lung cancer. *J Nucl Med.* 1999;40:556–565.
9. Reske SN, Grillenberger KG, Glatting G, et al. Overexpression of glucose transporter 1 and increased FDG uptake in pancreatic carcinoma. *J Nucl Med.* 1997;38:1344–1348.
10. Brown RS, Wahl RL. Overexpression of Glut-1 glucose transporter in human breast cancer: an immunohistochemical study. *Cancer.* 1993;72:2979–2985.
11. Boado RJ, Black KL, Pardridge WM. Gene expression of Glut-3 and Glut-1 glucose transporters in human brain tumors. *Brain Res Mol Brain Res.* 1994;27: 51–57.
12. Younes M, Brown RW, Stephenson M, Gondo M, Cagle PT. Overexpression of Glut-1 and Glut-3 in stage I nonsmall cell lung carcinoma is associated with poor survival. *Cancer.* 1997;80:1046–1051.
13. Suzuki T, Iwazaki A, Katagiri H, et al. Enhanced expression of glucose transporter Glut-3 in tumorigenic HeLa cell hybrids associated with tumor suppressor dysfunction. *Eur J Biochem.* 1999;262:534–540.
14. Aloj L, Caracó C, Jagoda E, Eckelman WC, Neumann RD. Glut-1 and hexokinase expression: relationship with 2-fluoro-2-deoxy-D-glucose uptake in A431 and T47D cells in culture. *Cancer Res.* 1999;59:4709–4714.
15. Kubota R, Yamada S, Kubota K, Ishiwata K, Tamahashi N, Ido T. Intratumoral distribution of fluorine-18-fluorodeoxyglucose in vivo: high accumulation in macrophages and granulation tissues studied by microautoradiography. *J Nucl Med.* 1992;33:1972–1980.
16. Kubota R, Kubota K, Yamada S, Tada M, Ido T, Tamahashi N. Microautoradiographic study for the differentiation of intratumoral macrophages, granulation tissues and cancer cells by the dynamics of fluorine-18-fluorodeoxyglucose uptake. *J Nucl Med.* 1994;35:104–112.
17. Brown RS, Leung JY, Fisher SJ, Frey KA, Ethier SP, Wahl RL. Intratumoral distribution of tritiated fluorodeoxyglucose in breast carcinoma. I. Are inflammatory cells important? *J Nucl Med.* 1995;36:1854–1861.
18. Kubota R, Kubota K, Yamada S, Tada M, Ido T, Tamahashi N. Active and passive mechanisms of [fluorine-18]fluorodeoxyglucose uptake by proliferating and prenecrotic cancer cells in vivo: a microautoradiographic study. *J Nucl Med.* 1994;35:1067–1075.
19. Kubota R, Kubota K, Yamada S, et al. Methionine uptake by tumor tissue: a microautoradiographic comparison with FDG. *J Nucl Med.* 1995;36:484–492.
20. Reinhardt MJ, Kubota K, Yamada S, Iwata R, Yaegashi H. Assessment of cancer recurrence in residual tumors after fractionated radiotherapy: a comparison of fluorodeoxyglucose, L-methionine and thymidine. *J Nucl Med.* 1997;38:280–287.
21. Zhao S, Kuge Y, Tsukamoto E, et al. Effects of insulin and glucose loading on FDG uptake in experimental malignant tumours and inflammatory lesions. *Eur J Nucl Med.* 2001;28:730–735.
22. Toorongian SA, Mulholland GK, Jewett DM, Bachelor MA, Kilbourn MR. Routine production of 2-deoxy-2-[^{18}F]fluoro-D-glucose by direct nucleophilic exchange on a quaternary 4-aminopyridinium resin. *Nucl Med Biol.* 1990;17: 273–279.
23. Zhao S, Kuge Y, Tsukamoto E, et al. Fluorodeoxyglucose uptake and glucose transporter expression in experimental inflammatory lesions and malignant tumours: effects of insulin and glucose loading. *Nucl Med Commun.* 2002;23:545–550.

24. Toyama H, Ichise M, Liow JS, et al. Absolute quantification of regional cerebral glucose utilization in mice by ^{18}F-FDG small animal PET scanning and 2-^{14}C-DG autoradiography. *J Nucl Med.* 2004;45:1398–1405.
25. Higashi T, Saga T, Nakamoto Y, et al. Relationship between retention index in dual-phase ^{18}F-FDG PET, and hexokinase-II and glucose transporter-1 expression in pancreatic cancer. *J Nucl Med.* 2002;43:173–180.
26. Zhong H, De Marzo AM, Laughner E, et al. Overexpression of hypoxia-inducible factor 1α in common human cancers and their metastases. *Cancer Res.* 1999;59: 5830–5835.
27. Higashi T, Tamaki N, Honda T, et al. Expression of glucose transporters in human pancreatic tumors compared with increased FDG accumulation in PET study. *J Nucl Med.* 1997;38:1337–1344.
28. Mochizuki T, Tsukamoto E, Kuge Y, et al. FDG uptake and glucose transporter subtype expressions in experimental tumor and inflammation models. *J Nucl Med.* 2001;42:1551–1555.
29. Bos R, Zhong H, Hanrahan CF, et al. Levels of hypoxia-inducible factor-1α during breast carcinogenesis. *J Natl Cancer Inst.* 2001;93:309–314.
30. Brown RS, Leung JY, Fisher SJ, Frey KA, Ethier SP, Wahl RL. Intratumoral distribution of tritiated-FDG in breast carcinoma: correlation between Glut-1 expression and FDG uptake. *J Nucl Med.* 1996;37:1042–1047.
31. Dang CV, Semenza GL. Oncogenic alterations of metabolism. *Trends Biochem Sci.* 1999;24:68–72.
32. Clavo AC, Brown RS, Wahl RL. Fluorodeoxyglucose uptake in human cancer cell lines is increased by hypoxia. *J Nucl Med.* 1995;36:1625–1632.
33. Dearling JL, Flynn AA, Sutcliffe-Goulden J, et al. Analysis of the regional uptake of radiolabeled deoxyglucose analogs in human tumor xenografts. *J Nucl Med.* 2004;45:101–107.
34. Flier JS, Mueckler MM, Usher P, Lodish HF. Elevated levels of glucose transport and transporter messenger RNA are induced by *ras* or *src* oncogenes. *Science.* 1987;235:1492–1495.
35. Birnbaum MJ, Haspel HC, Rosen OM. Transformation of rat fibroblasts by FSV rapidly increases glucose transporter gene transcription. *Science.* 1987;235:1495–1498.
36. Smith TA. Mammalian hexokinases and their abnormal expression in cancer. *Br J Biomed Sci.* 2000;57:170–178.
37. Bell HS, Whittle IR, Walker M, Leaver HA, Wharton SB. The development of necrosis and apoptosis in glioma: experimental findings using spheroid culture systems. *Neuropathol Appl Neurobiol.* 2001;27:291–304.
38. Bos R, van Der Hoeven JJ, van Der Wall E, et al. Biologic correlates of ^{18}fluorodeoxyglucose uptake in human breast cancer measured by positron emission tomography. *J Clin Oncol.* 2002;20:379–387.
39. Oshida M, Uno K, Suzuki M, et al. Predicting the prognoses of breast carcinoma patients with positron emission tomography using 2-deoxy-2-fluoro[^{18}F]-D-glucose. *Cancer.* 1998;82:2227–2234.
40. Lucignani G, Jereczek-Fossa BA, Orecchia R. The role of molecular imaging in precision radiation therapy for target definition, treatment planning optimisation and quality control. *Eur J Nucl Med Mol Imaging.* 2004;31:1059–1063.

J. Radiat. Res., 46, 93–102 (2005)

Regular Paper

Real-time Imaging of Hypoxia-inducible Factor-1 Activity in Tumor Xenografts

Junye LIU[1,2], Runjiang QU[1,2], Masakazu OGURA[1], Toru SHIBATA[1], Hiroshi HARADA[1,3]* and Masahiro HIRAOKA[1]

Hypoxia/Hypoxia-inducible factor-1 (HIF-1)/Hypoxia-response element (HRE)/Pimonidazole/Destabilized Enhanced GFP (d2EGFP).

Hypoxia-inducible factor-1 (HIF-1) is responsible for various gene expressions related to tumor malignancy, such as metastasis, invasion and angiogenesis. Therefore, monitoring HIF-1 activity in solid tumors is becoming increasingly important in clinical and basic studies. To establish a convenient system for visualizing HIF-1 activity in tumor xenografts, we employed a promoter consisting of five copies of hypoxia response elements (5HRE), whose activity depends on HIF-1, and used a derivative of green fluorescence protein (d2EGFP) as a reporter gene. A human melanoma cell line, Be11, which contains the 5HRE-d2EGFP gene, showed fluorescence in response to hypoxia. The fluorescent intensity correlated inversely with the surrounding oxygen tension, and was time-dependent for the hypoxic treatment. Reoxygenation resulted in a rapid decrease in fluorescence due to the signal sequence for protein degradation encoded in d2EGFP, which enabled monitoring of HIF-1 activity in real-time. Heterogeneous fluorescence was observed in the solid tumor of a non-sacrificed tumor-bearing mouse. Immunohistochemical analysis confirmed that d2EGFP-expressing regions overlapped with the ones stained with a hypoxia marker, pimonidazole. These results suggest that the 5HRE-d2EGFP gene is suitable for the real-time imaging of HIF-1-activating cells *in vivo*, due to the short half-life of the d2EGFP protein as well as the specificity of the 5HRE promoter for HIF-1 activity.

INTRODUCTION

The rapid proliferation and high metabolic demands of cancer cells cause a reduction in oxygen tension to below physiological levels, which is a typical feature of solid tumors and is known as tumor hypoxia.[1,2] In hypoxic tumor cells, a transcriptional factor, hypoxia-inducible factor-1 (HIF-1), induces various kinds of gene expression related to angiogenesis[3] and glycolysis[4], and appears to play a critical role in the development of invasive and metastatic properties.[5] Moreover, HIF-1 activity is associated with the resistance of tumor cells against radiotherapy as well as chemotherapy.[6,7] For example, it has been demonstrated that ionizing radiation (IR) treatment up-regulates HIF-1 activity and induces vascular endothelial growth factor (VEGF) gene expression in tumor cells, which then leads to radioresistance of endothelial cells and eventually to radioresistance of the tumor cells themselves.[8] In addition, significant associations between HIF-1 activity and patient mortality have been reported in clinical studies of brain[9], breast[10,11], cervix[12], oropharynx[13], ovarian cancer[14] *etc.*

HIF-1 is a heterodimeric transcriptional factor composed of α subunit (HIF-1α) and β subunit (HIF-1β), which is also known as ARNT (aryl hydrocarbon receptor nuclear translocator).[15] HIF-1α expression is regulated in an oxygen-dependent manner at the post-translational level and is responsible for the regulation of HIF-1 activity.[16] Under aerobic conditions, the proline residues, Pro-402 and Pro-564, in the oxygen dependent degradation (ODD) domain of HIF-1α protein are hydroxylated by prolyl hydroxylase-domain protein 1-3 (PHD1-3).[17,18] The modified HIF-1α protein is recognized as a target for ubiquitylation by E3 ubiquitin-protein ligases containing the von Hippel-Lindau tumor suppressor protein (pVHL).[17,18] Consequently, the ubiquitylated HIF-1α is degraded by the 26S proteasome.[17,18] On the other hand, the rate of prolyl hydroxylation decreases under

*Corresponding author: Phone: +81-75-751-3417,
Fax: +81-75-751-9749,
E-mail: hharada@kuhp.kyoto-u.ac.jp
[1]Department of Therapeutic Radiology and Oncology, Kyoto University Graduate School of Medicine, Kyoto, Japan; [2]Department of Radiation Medicine, Fourth Military Medical University, Xi'an, China; [3]Horizontal Medical Research Organization, Kyoto University Graduate School of Medicine, Kyoto, Japan.
Junye LIU and Runjiang QU contributed equally to this work.

hypoxic condition and VHL cannot recognize HIF-1α as a target, resulting in a reduced rate of degradation.[17,18] The stabilized HIF-1α interacts with the constitutively expressed HIF-1β protein and induces the expression of certain genes such as VEGF[3], glycolytic enzyme[4] and erythropoietin.[19] The induction of these genes is triggered by the interaction of HIF-1 with its cognate DNA recognition site, that is, the hypoxia-response element (HRE).[3,20] Previously, Shibata *et al.* developed an artificial hypoxia-inducible promoter system using five copies of HRE (5HRE) derived from the VEGF promoter and the human cytomegalovirus minimal promoter (CMVmp), and demonstrated that the 5HRE promoter increased gene expression by a factor of more than 500 under hypoxic conditions *in vitro*.[21,22]

In the process of developing radiosensitizers, 2-nitroimidazole derivatives have been found to accumulate in hypoxic cells of solid tumors. Consequently, some methods to obtain quantitative or qualitative data about tumor hypoxia have been developed, and suitably labeled 2-nitroimidazole analogues have been utilized to develop a variety of non-invasive monitoring systems for tumor hypoxia, *e.g.* magnetic resonance spectroscopy (MRS)[23,24], positron emission tomography (PET)[25] and single photon electron capture tomography (SPECT).[25] Pimonidazole, a well-known hypoxia marker, is also a 2-nitroimidazole derivative and has been developed for the immunohistochemical analysis of tumor specimens.[26,27] Polarographic microelectrodes can directly record the oxygen status of tumor tissues and have therefore been widely used in clinical practice for cancer patients.[27] Although all of these methods yield detailed information about tumor hypoxia, they do not accurately reflect HIF-1 activity because HIF-1 activation is caused by not only intratumoral hypoxia but also by genetic alterations, such as gain-of-function mutations in oncogenes and loss-of-function mutations in tumor-suppressor genes.[28] Moveover, growth factors and cytokines stimulate HIF-1α synthesis via the oxygen-independent activation of phosphatidylinositol 3-kinase (PI3K)[29,30] or mitogen-activated protein kinase (MAPK) pathways.[31] VHL mutation also leads to over expression of the HIF-1α protein.[32] Therefore, lack of a routine, easy and dynamic method to monitor HIF-1 activity in solid tumors remains a major problem.

In the present study, we developed a suitable and convenient system to monitor HIF-1 activity in real-time in tumor xenografts by using the 5HRE promoter.[21,22] Destabilized Enhanced GFP (d2EGFP) was chosen as the reporter gene because it can be detected without any substrate or cofactor, and especially because the half-life of d2EGFP is reduced to less than 2 hours. Such short half-life is due to the residues 422–461 of mouse ornithine decarboxylase protein (MODC domain) fused in d2EGFP protein, and makes it possible to observe HIF-1 activity in real-time.[33] We were consequently able to demonstrate that d2EGFP fluorescence is observed *in vitro* only under hypoxic conditions and *in vivo* in the regions stained with the hypoxia marker.

MATERIALS AND METHODS

DNA constructs

The DNA fragments encoding EGFP and d2EGFP were inserted between the NcoI and NotI recognition sites of the pEF/myc/cyto vector (Invitrogen, Carlsbad, CA) to construct the plasmids pEF/EGFP and pEF/d2EGFP, respectively. In addition, the DNA fragment of the 5HRE-hCMVmp enhancer/promoter[22] was inserted between the KpnI and NcoI sites of pEF/EGFP and pEF/d2EGFP to construct the plasmids p5HRE-EGFP and p5HRE-d2EGFP, respectively. To construct the plasmid, pCMV-d2EGFP, the DNA fragment of the 5HRE-hCMVmp enhancer/promoter of p5HRE-d2EGFP was substituted for that of the intact CMV promoter.[22]

Cell culture and transfection

The human melanoma cell line Be11[34] (the gift from Dr. Oya) was cultured in 20% FCS-MEM-1. To establish the stable transfectants, the cells were seeded on a 60mm culture dish and transfected with 5 μg of pCMV-d2EGFP, p5HRE-EGFP or p5HRE-d2EGFP by using the Superfect Transfection Reagent (QIAGEN, Valencia, CA), according to the manufacture's instructions. Three hours after the transfection, the culture medium was changed to the medium containing 800 μg/ml of G418 disulfate (Nacalai Tesque, Kyoto, Japan), an antibiotic to select the stable transfectant, and the cells were cultured for an additional 2 weeks. With the aid of a fluorescent microscope with a 488 / 510 filter, a stable transfectant with strong fluorescence was isolated from the cells transfected with pCMV-d2EGFP plasmid. The stable transfectant with p5HRE-d2EGFP, on the other hand, was treated under hypoxic conditions (0.02%) for 20 hours before being isolated.

Hypoxia treatment and reoxygenation

Cells were treated under various hypoxic conditions. In one procedure, 90% N_2, 5% H_2 and 5% CO_2 with a palladium catalyst were used in an Environment Chamber (Sheldon Manufacturing, Inc., Cornelius, OR). In another, the cells were treated in pre-warmed aluminum chambers by means of exhausting and gassing with 95% N_2 and 5% CO_2 for various cycles to produce oxygen concentrations of 2%, 0.2%, 0.02% and <0.01%. After the hypoxic treatment (0.02% O_2) for 20 hours, the cells were cultured in the incubator with 95% air and 5% CO_2 for the times indicated in each figures to reoxygenate the cells.

Flow cytometry analysis

Green fluorescence was analyzed with a flow cytometer (Becton Dickinson, San Jose, CA), and the data were processed with CellQuest software (Becton Dickinson). Histograms of GFP were plotted with the log scale for GFP fluo-

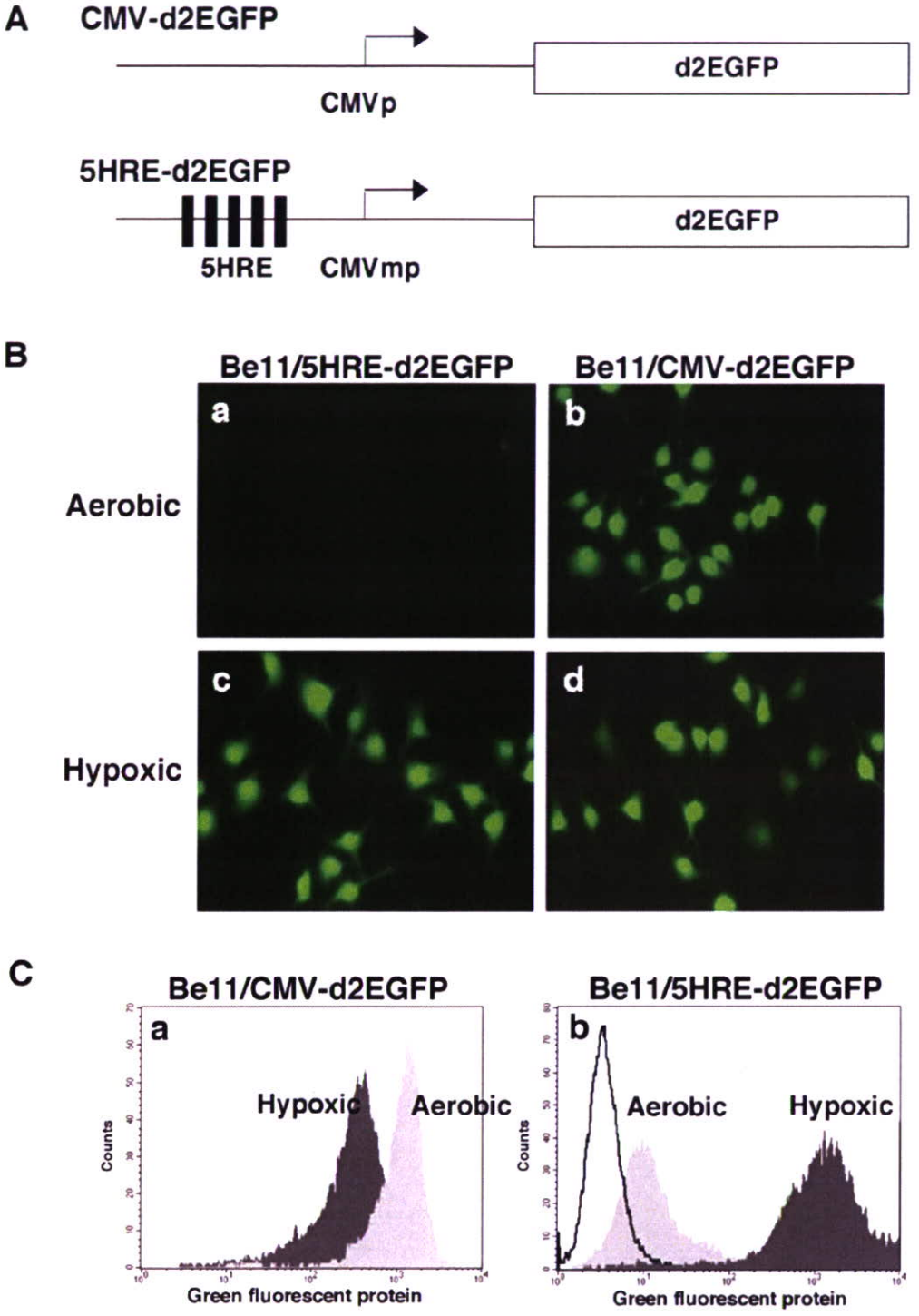

Fig. 1. Hypoxia-responsible d2EGFP expression in Be11/5HRE-d2EGFP stable transfectant. **(A)** Schematic diagrams of the CMV-d2EGFP gene (top) and the 5HRE-d2EGFP gene (bottom). **(B)** Both stable transfectants Be11/5HRE-d2EGFP (a, c) and Be11/CMV-d2EGFP (b, d) were treated under hypoxic condition (0.02% O_2) for 20 hours, and reoxygenated for 4 hours. **(C)** After the same treatment as described in (B), Be11/CMV-d2EGFP (a) and Be11/5HRE-d2EGFP (b) were subjected to FACS analysis and histograms of their fluorescent intensity are shown.

rescence and the results were recorded as means of the middle of the peaks.

Immunohistochemical analysis

Stable transfectants of Be11 with pCMV-d2EGFP or p5HRE-d2EGFP (10^6 cells in 100 μl of PBS) were subcutaneously (s.c.) injected into the flank or leg of 6–8 weeks nude mice (BALB/c nu/nu; CLEA Japan, Inc., Tokyo, Japan). When the tumor diameter exceeded 15 mm, the tumor bearing mice were intraperitoneally (i.p.) injected with pimonidazole hydrochloride[26,27] (60mg/kg), and 90 min later, the solid tumors were surgically removed and fixed in 10% Formalin Neutral Buffer Solution pH 7.4 (Wako Pure Chemical Industries, Osaka, Japan). Immunostaining for the detection of d2EGFP expression and hypoxic cells was carried out with the anti-GFP Ab (BD Living Color™ A.v. Peptide Antibody; Clontech, Franklin Lakes, NJ) and with anti-pimonidazole Ab (Hypoxyprobe-1 kit; Natural Pharmacia International, Inc., Belmont, MA), respectively, by the indirect immunoperoxidase method as described previously.[35] To calculate the percentage of pimonidazole-positive cells and d2EGFP-expressing cells in the Be11/5HRE-d2EGFP solid tumor, the corresponding pimonidazole-stained cells and d2EGFP-stained cells were quantified with NIH Image 1.63 software, and compared to the quantity of the whole tumor.

Fluorescent microscope analysis and imaging of HIF-1 activity in vivo

Microscopic analysis was conducted with an Olympus BX-60 microscope fitted with Olympus U-MWIB filter cubes (460–490 nm for excitation filter, 505–550 nm for dichroic filter and 515–550 for emission filter). Images were taken with a Sensys CCD Camera (Photometric, Livingston, UK). Blue color excitation light and yellow filters were used for the *in vivo* real-time imaging.

RESULTS

Hypoxia-inducible fluorescence from cells transfected with p5HRE-d2EGFP

To establish a convenient system to visualize the HIF-1 transcriptional activity in tumor xenografts in real-time, we first constructed the p5HRE-d2EGFP plasmid (Fig. 1A). A

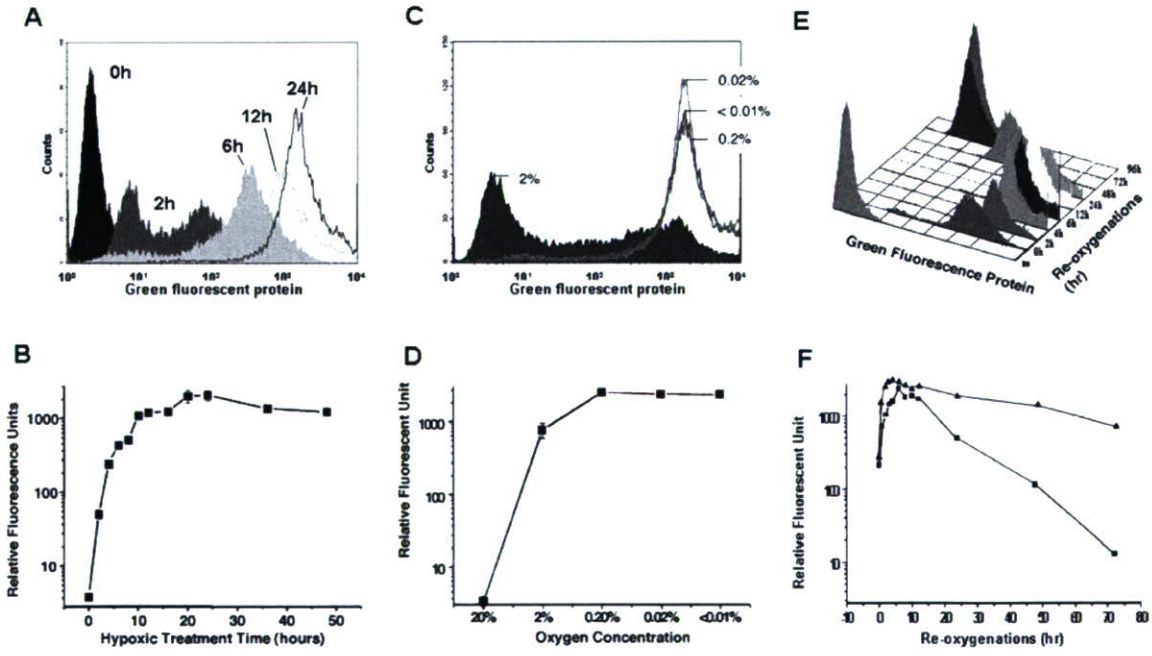

Fig. 2. Effects of various hypoxic treatments on d2EGFP fluorescence. **(A)** After hypoxic treatment (0.02% O_2) of various durations, fluorescent intensity of Be11/5HRE-d2EGFP stable transfectants was analyzed with FACS and is shown as a histogram. **(B)** Ratios of fluorescent intensity of the same cell preparations as in (A) to the intensity without hypoxic treatment are shown as relative fluorescence units. **(C)** After various hypoxic treatments (2%, 0.2%, 0.02% and <0.01%) for 20 hours, fluorescent intensity of Be11/5HRE-d2EGFP stable transfectants was analyzed and is shown as a histogram. **(D)** Ratios of fluorescent intensity of the cells after the same hypoxic treatments as in (C) to the intensity after aerobic treatment are shown as relative fluorescence units. **(E)** After hypoxic treatment (0.02% O_2) for 20 hours, Be11/5HRE-d2EGFP stable transfectants were reoxygenated for various durations and the fluorescent intensity was analyzed and is shown here as a histogram. **(F)** Ratios of fluorescent intensity of the cells after the same treatment as in (E) to the intensity after aerobic treatment are shown as relative fluorescence units. Be11/5HRE-EGFP stable transfectants (solid triangles), Be11/5HRE-d2EGFP stable transfectants (solid squares).

5HRE promoter was employed to induce reporter gene expression under the control of HIF-1 activity,[21,22] and d2EGFP was used as a reporter gene, because its half-life is reported to be somewhat less than 2 hours,[33] which we thought should enable us to observe HIF-1 activity in real-time. The human melanoma cell line Be11 was stably transfected with the plasmid p5HRE-d2EGFP, and a clone was isolated by taking advantage of the hypoxia-dependency of the d2EGFP expression (Fig. 1A). In addition, Be11, this time stably transfected with pCMV-d2EGFP plasmid, was established as a control with constitutive expression of d2EGFP (Fig. 1A). To confirm the occurrence of hypoxic induction, both stable transfectants were processed in 0.02% of oxygen concentration. The fluorescence microscopic examination clearly showed that Be11/5HRE-d2EGFP transfectants expressed negligible levels of fluorescence under aerobic conditions but adequate levels of fluorescence after hypoxic treatment (Fig. 1Ba and c). On the other hand, Be11/CMV-d2EGFP transfectants showed bright green fluorescence under both aerobic and hypoxic conditions (Fig. 1Bb and d).

FACS analysis also clearly showed fluorescent intensity in both cell lines (Fig. 1C). In the cell population of Be11/5HRE-d2EGFP transfectants, a more than 200-fold induction of d2EGFP fluorescence was observed after hypoxic treatment compared to after aerobic treatment (Fig. 1Cb), whereas constitutive fluorescence was observed after both aerobic and hypoxic treatment in the Be11/CMV-d2EGFP transfectants (Fig. 1Ca). These results indicate that the 5HRE-CMVmp promoter can be used as a specific and robust hypoxia-inducible promoter. Although hypoxic treatment itself seemed to somewhat diminish the brightness of the Be11/CMV-d2EGFP transfectants (Fig. 1Ca), such difference was hardly detectable by fluorescence microscopic analysis (Fig. 1Bb and d).

Effects of various hypoxic treatments on d2EGFP fluorescence

In order to analyze the effects of hypoxic treatment of various durations on fluorescent intensity, Be11/5HRE-d2EGFP transfectants were treated under hypoxic conditions for 0, 2, 6, 12, and 24 hours, after which the green fluorescence was monitored by means of FACS analysis. Even after 2 hours of hypoxic treatment, fluorescence was detected with fluorescent microscopic as well as with FACS analysis (Fig. 2A and data not shown). Increases in both fluorescent intensity and number of fluorescent cells depended on the duration of hypoxic treatment up to 24 hours, after which saturation levels were reached (Fig. 2A and B).

To assess the oxygen concentration required for inducing d2EGFP expression, Be11/5HRE-d2EGFP cells were treated for 20 hours with various oxygen concentrations, that is, <0.01%, 0.02%, 0.2% and 2%. FACS analysis showed that d2EGFP expression increased when the oxygen concentra-

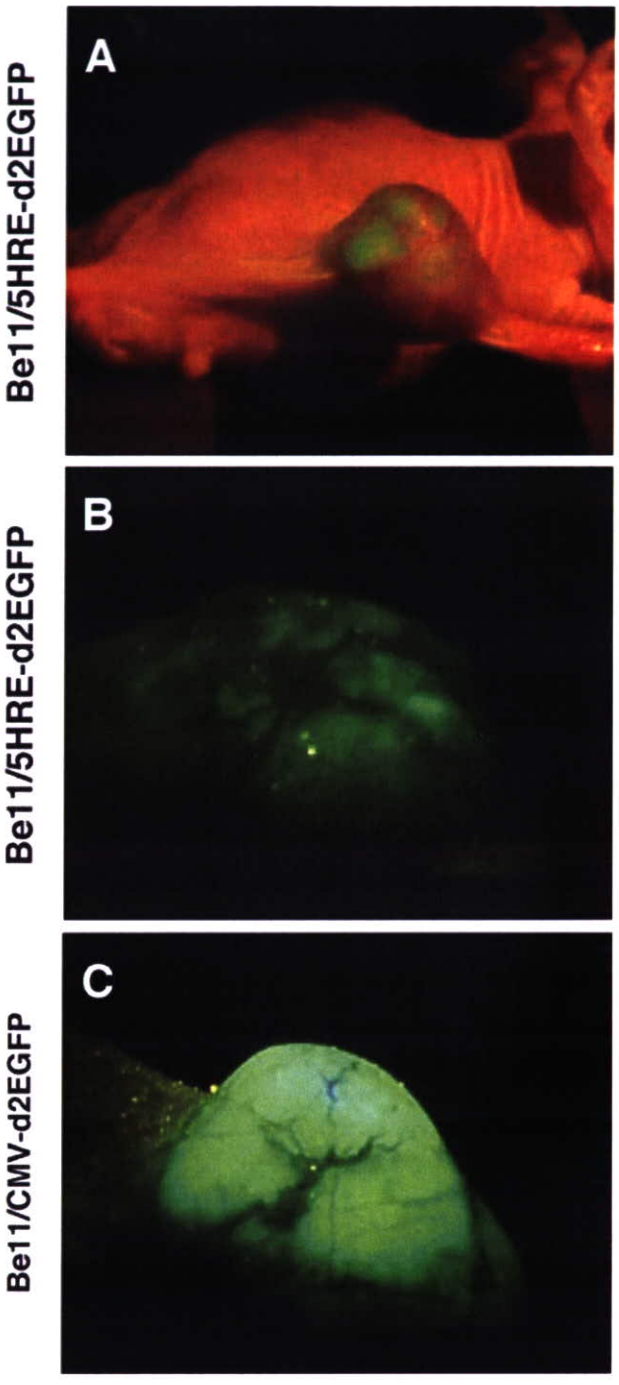

Fig. 3. Real-time imaging of HIF-1 activity in the Be11/5HRE-d2EGFP tumor xenograft. **(A)**, **(B)** Heterogeneous fluorescence in the tumor xenograft with Be11/5HRE-d2EGFP cells was detected by means of blue excitation light and a yellow filter. **(C)** Homogeneous fluorescence in the tumor xenograft with Be11/CMV-d2EGFP cells was used as control.

tion was reduced from 20% to 0.2%, and maintained a high expression level from 0.2% to anaerobia (<0.01%) (Fig. 2C and D). Even at the 2% oxygen concentration, fluorescent intensity increased almost 1,000 times compared to the one at 20% oxygen concentration (Fig. 2D), and could be detected directly with the fluorescence microscope (data not shown).

Next we analyzed the effect of reoxygenation on d2EGFP fluorescence, because oxygen molecules are reported to be necessary for chromophore formation of GFP and its derivatives.[36] Be11/5HRE-d2EGFP cells were treated under hypoxic conditions (0.02% O_2) for 20 hours, and reoxygenated for various lengths of time in the incubator with 95% air and 5% CO_2. The hypoxic treatment even without any reoxygenation enhanced fluorescence by a factor of more than 200 compared to that observed under aerobic conditions (Fig. 2E and F). Reoxygenation for 4 hours resulted in a sharp and high peak of fluorescence, after which the fluorescence levels decreased dramatically. To examine the effect of the MODC domain fused in d2EGFP on protein stability, we established the Be11/5HRE-EGFP cells, in which expression of the EGFP protein (without MODC domain) was controlled by the 5HRE promoter. When the Be11/5HRE-EGFP cells were subjected to the same experiment as described above, they showed more stable fluorescence than the Be11/5HRE-d2EGFP cells during the observation period (Fig. 2F). These results clearly demonstrate that the decrease in the fluorescence of Be11/5HRE-d2EGFP was due to the MODC domain of the d2EGFP protein.

Real-time imaging of HIF-1 transcriptional activity in tumor xenograft

In order to visualize the HIF-1 transcriptional activity in a solid tumor in a living mouse, Be11/5HRE-d2EGFP cells were s.c. inoculated into nude mice. One month after the implantation, these cells formed solid tumors with diameter of more than 15 mm. Real-time imaging under the blue exci-

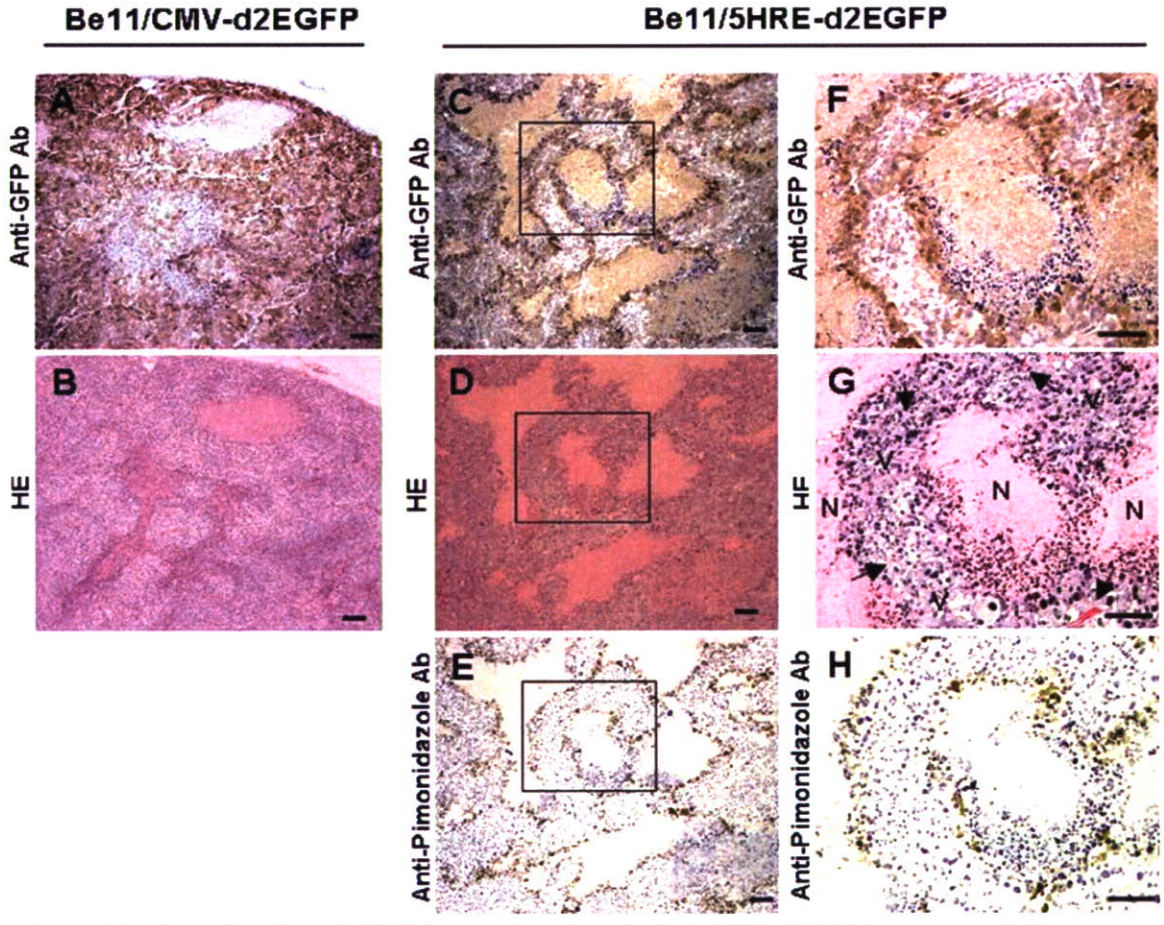

Fig. 4. Immunohistochemical analysis of d2EGFP-expressing cells in the Be11/5HRE-d2EGFP tumor xenograft. Tumor xenografts of Be11/CMV-d2EGFP cells (**A** and **B**) and Be11/5HRE-d2EGFP cells (**C-H**) were stained with anti-GFP Ab (**A, C** and **F**), HE (**B, D** and **G**) and anti-pimonidazole Ab (**E** and **H**). F, G and H show higher magnifications of the square areas in C, D and E, respectively. Bar = 100 μm. N = necrotic tumor tissue; V = well-oxygenated viable tumor tissue; arrow = blood vessel.

tation light showed heterogeneous, partition-dependent and weak green fluorescence in the tumor xenograft with Be11/5HRE-d2EGFP cells (Fig. 3A and B). In comparison, tumor xenografts with Be11/CMV-d2EGFP cells showed strong and homogeneous green fluorescence (Fig. 3C). No fluorescence was observed in the parental Be11 tumor (data not shown).

Characterization of GFP-expressing cells by immunohistochemical analysis

HIF-1 activation is induced by not only intratumoral hypoxia but also the other stimuli.[28–32] To determine, therefore, whether hypoxic stimuli definitely up-regulated the 5HRE-promoter activity in our *in vivo* study, the regions expressing d2EGFP in the solid tumor were compared to those stained with the hypoxic marker pimonidazole.[26,27] In the Be11/CMV-d2EGFP solid tumor, homogeneous and strong expressions of d2EGFP proteins were detected with the anti-GFP Ab, which recognizes all of GFP derivatives including d2EGFP (Fig. 4A). HE-stained section of Be11/CMV-d2EGFP xenograft revealed that the d2EGFP-expressing cells were in the viable regions (Fig. 4B). On the other hand, heterogeneous expressions of d2EGFP were observed in the tumor xenografts with Be11/5HRE-d2EGFP cells (Fig. 4C). The d2EGFP-positive cells were located in the boundary area between the well-oxygenated viable regions and the necrotic regions (Fig. 4C and D). Similar regions in the Be11/5HRE-d2EGFP tumor also stained with anti-pimonidazole Ab, (Fig. 4E).

Higher magnifications of the square areas in Fig. 4C, 4D and 4E are shown as Fig. 4F, 4G and 4H, respectively. In the HE-stained specimen, red blood cells clearly showed the location of tumor blood vessels (Fig. 4G), which were surrounded by viable tumor cells in direct proximity, and moreover by necrotic tumor cells at a greater distance. To be precise, the necrotic regions were located more than 100 μm from the blood vessels. In addition to the HE-stained specimens, the higher-magnified images stained with anti-GFP Ab clearly demonstrated that the d2EGFP-expressing cells were located about 100 μm from the tumor blood vessels (Fig. 4F). Finally, the staining pattern obtained with anti-GFP Ab was very similar to that produced by the hypoxia marker pimonidazole (Fig 4F and H). These results strongly suggest that the 5HRE-system induces d2EGFP expressions in hypoxic tumor cells.

In the specimens stained with anti-GFP Ab and anti-pimonidazole Ab, it was also clear that more cells were stained with the former than with the latter. For quantification, both specimens were analyzed with NIH Image 1.63 software. The percentage of pimonidazole-positive cells in the whole solid tumor was $9.2 \pm 3.8\%$ ($n = 5$), while that of d2EGFP-expressing cells in the whole solid tumor was significantly higher, $22.7 \pm 6.1\%$ ($n = 5$; $p < 0.01$).

DISCUSSION

HIF-1 induces various kinds of hypoxia-responsive gene expressions, which are related to the malignant phenotype of tumor cells, such as angiogenesis, metastasis, invasion and evasion of apoptosis.[3–5] The lack of a technique that allows for convenient imaging of HIF-1 transcriptional activity therefore remains as one of the problems for basic research aiming at the development of anticancer drugs in cancer treatment. In order to address this issue, we developed an imaging system using both an HIF-1-responsive promoter and a specific reporter protein. Shibata *et al.* examined various combinations of HRE and promoters to achieve higher responsiveness of promoter activity to hypoxic stress, and demonstrated that the combination of 5HRE and a CMVmp induces 500 fold more gene expression under hypoxic conditions than under aerobic conditions. Moreover, the expression level under hypoxic conditions is almost same as the one by the intact CMV promoter.[22] We therefore employed the 5HRE-hCMVmp enhancer/promoter system for the study presented here. In agreement with previously reported results,[22] only negligible levels of reporter expression were observed under aerobic conditions but these levels became clearly detectable after hypoxic treatment. For this reason, the 5HRE enhancer/promoter met our requirements better than any other regulatory systems.

We chose a derivative of GFP protein as the reporter gene because no additional cofactor or substrate is needed for its visualization. Attention must be paid, however, to applying GFP derivatives to *in vivo* imaging because anoxic conditions inhibit chromophore formation.[36] In fact, we observed in the FACS analyses that hypoxic treatment itself seemed to diminish the brightness of the Be11/CMV-d2EGFP transfectants somewhat (Fig. 1Ca), and that d2EGFP fluorescence increased after reoxygenation (Fig. 2E and F). But when we treated the cells with the translation inhibitor, cyclohexamide, just after the hypoxic treatment, the d2EGFP signal did not increase after reoxygenation (data not shown). This finding suggests that the increase in fluorescence after reoxygenation was not mainly the result of chromophore formation but of translation. We can therefore conclude that chromophore formation was not significantly inhibited in our experimental setting. Additionally, such small differences in fluorescent intensity were hardly detectable with fluorescence microscopic analysis (Fig. 1Bb and d). Thus, there seemed to be no serious obstacles to employing d2EGFP as a reporter for our purpose.

The 5HRE enhancer/promoter system has been used to analyze the effect of x-ray irradiation on tumor reoxygenation as well as on subsequent HIF-1 activation.[8] The HIF-1-mediated promoter with eight copies of HRE has also been used to develop a novel PET imaging system.[37] In both cases, however, assessment in real-time seemed to be difficult,

because the reporter proteins were so stable[33] that some of them may have remained in the cells after reoxygenation. The reason why we choose d2EGFP rather than the other GFP derivatives was the short half-life of the protein, which is caused by the MODC domain fused in it.[33] In fact, we were able to demonstrate that d2EGFP fluorescence has a more rapid turnover than that of EGFP (Fig. 2F). Moreover, when we treated the cells with cyclohexamide just after the hypoxic treatment and just before reoxygenation, the d2EGFP fluorescence disappeared within 2 hours (data not shown). This MODC activity enabled us to assess HIF-1 activity in solid tumors in real-time.

Be11/CMV-d2EGFP showed homogeneous fluorescence in the whole tumor, while heterogeneous occurrence of green fluorescence was directly visualized in tumor xenografts inoculated with Be11/5HRE-d2EGFP cells. Our *in vitro* study enabled us to estimate to some extent the hypoxic status in the solid tumor. As Be11/5HRE-d2EGFP expressed detectable amounts of fluorescence in response to different hypoxic stimuli, e.g. 0.02% O_2 for 2 hours and <2% O_2 for 20 hours, we can assume that the fluorescent cells in the solid tumors were exposed to at least these conditions. At this time, however, an accurate assessment of tumor hypoxia with this method alone is not possible. For instance, it was difficult to distinguish the acute hypoxia from the chronic one. Moreover, we might not have visualized the acute hypoxia, but chronic one alone, because most gene expressions take a certain time. Therefore, combining our method with computer based image analysis and/or flow cytometry analysis can be expected to expand the efficacy and application of 5HRE-d2EGFP as an imaging system.

Immunohistochemical analysis clearly showed that the d2EGFP-expressing cells are located at a distance of about 100 μm from the tumor blood vessels, and the staining pattern is almost the same as the one obtained with anti-pimonidazole Ab. These results suggest that the 5HRE enhancer/promoter induces d2EGFP expressions in response to hypoxic stimuli in the solid tumor. However, more highly magnified images showed that more cells are stained with anti-GFP Ab than with anti-pimonidazole Ab in the boundary area between viable and necrotic regions (Fig. 4F and H). The quantitative analysis using NIH Image 1.63 software also clearly showed that there were certainly more GFP-expressing cells than pimonidazole-positive cells. Although these results might have been caused simply by the different sensitivities of the Abs, it is also possible that the HIF-1 activity is up-regulated by another regulatory pathway independent of hypoxia. The up-regulation of HIF-1α activity has been observed even under normoxic conditions in renal carcinoma cells, in which the von Hippel-Lindau tumor suppressor gene had lost its function.[38] Furthermore, HIF-1 activity increases when the PI3K/AKT signaling pathway is activated.[30] Regardless of the HIF-1-activating mechanisms, the 5HRE-d2EGFP system can reflect the HIF-1 activity, so that this system can be used for monitoring HIF-1 activity in real-time *in vivo*.

It has been reported that HIF-2 as well as HIF-1 regulates gene expression of VEGF, glycolytic enzymes and other HRE-driven genes in response to hypoxia.[39] Although HIF-2 plays some important roles in physiological stress response, the details of its mechanism and how it differs from that of the HIF-1 pathway remain unknown. To examine whether the 5HRE enhancer/promoter system is regulated by HIF-2 activity, too, we assessed its hypoxia responsiveness by using a squamous cell carcinoma cell line, in which the HIF-1α gene was mutated, and found evidence of the HIF-2-dependency of the 5HRE system. (in preparation). These findings indicate that this monitoring method can be used to analyze details of the activities of the HIF family *in vivo*. Moreover, this method can be expected to contribute to the development of HIFs-targeting drugs,[28] such as YC-1[40] and TOP3.[6,35,41]

ACKNOWLEDGEMENTS

We are grateful to Drs. N. Oya (Kumamoto University, Kumamoto, Japan) and S. Kizaka-Kondoh (Kyoto University, Kyoto, Japan) for discussion, and A. Morinibu for skilled technical assistance. This work was supported by research grants from the Ministry of Education, Science, Sports, and culture of Japan.

REFERENCES

1. Dang, C.V. and Semenza, G. L. (1999) Oncogenic alterations of metabolism. Trends Biochem. Sci. **24**: 68–72.
2. Vaupel, P., Kallinowski, F. and Okunieff, P. (1989) Blood flow, oxygen and nutrient supply, and metabolic microenvironment of human tumors: a review. Cancer Res. **49**: 6449–6465
3. Forsythe, J. A., Jiang, B. H., Iyer, N. V., Agani, F., Leung, S. W., Koos, R. D. and Semenza, G. L. (1996) Activation of vascular endothelial growth factor gene transcription by hypoxia-inducible factor 1. Mol. Cell Biol. **16**: 4604–4613.
4. Semenza, G. L., Roth, P. H., Fang, H. M. and Wang, G. L. (1994) Transcriptional regulation of genes encoding glycolytic enzymes by hypoxia-inducible factor 1. J. Biol. Chem. **269**: 23757–23763.
5. Zhong, H., De Marzo, A. M., Laughner, E., Lim, M., Hilton, D. A., Zagzag, D., Buechler, P., Isaacs, W. B., Semenza, G. L. and Simons, J. W. (1999) Overexpression of hypoxia-inducible factor 1alpha in common human cancers and their metastases. Cancer Res. **59**: 5830–5835.
6. Kizaka-Kondoh, S., Inoue, M., Harada, H. and Hiraoka, M. (2003) Tumor hypoxia: A target for selective cancer therapy. Cancer Sci. 94, 1021–1028.
7. Brown, J. M. (1999) The hypoxic cell: a target for selective cancer therapy--eighteenth Bruce F. Cain Memorial Award lecture. Cancer Res. **59**: 5863–5870.
8. Moeller, B. J., Cao, Y., Li, C. Y. and Dewhirst, M. W. (2004)

Radiation activates HIF-1 to regulate vascular radiosensitivity in tumors: role of reoxygenation, free radicals, and stress granules. Cancer Cell. **5**: 429–441.
9. Birner, P., Gatterbauer, B., Oberhuber, G., Schindl, M., Rossler, K., Prodinger, A., Budka, H. and Hainfellner, J. A. (2001) Expression of hypoxia-inducible factor-1 alpha in oligodendrogliomas: its impact on prognosis and on neoangiogenesis. Cancer. **92**: 165–171.
10. Schindl, M., Schoppmann, S. F., Samonigg, H., Hausmaninger, H., Kwasny, W., Gnant, M., Jakesz, R., Kubista, E., Birner, P. and Oberhuber, G.; Austrian Breast and Colorectal Cancer Study Group. (2002) Overexpression of hypoxia-inducible factor 1alpha is associated with an unfavorable prognosis in lymph node-positive breast cancer. Clin. Cancer Res. **8**: 1831–1837.
11. Bos, R., van der Groep, P., Greijer, A. E., Shvarts, A., Meijer, S., Pinedo, H. M., Semenza, G. L., van Diest, P. J. and van der Wall, E. (2003) Levels of hypoxia-inducible factor-1alpha independently predict prognosis in patients with lymph node negative breast carcinoma. Cancer. **97**: 1573–1581.
12. Birner, P., Schindl, M., Obermair, A., Plank, C., Breitenecker, G. and Oberhuber, G. (2000) Overexpression of hypoxia-inducible factor 1alpha is a marker for an unfavorable prognosis in early-stage invasive cervical cancer. Cancer Res. **60**: 4693–4696.
13. Aebersold, D. M., Burri, P., Beer, K. T., Laissue, J., Djonov, V., Greiner, R. H. and Semenza, G. L. (2001) Expression of hypoxia-inducible factor-1alpha: a novel predictive and prognostic parameter in the radiotherapy of oropharyngeal cancer. Cancer Res. **61**: 2911–2916.
14. Birner, P., Schindl, M., Obermair, A., Breitenecker, G. and Oberhuber, G. (2001) Expression of hypoxia-inducible factor 1alpha in epithelial ovarian tumors: its impact on prognosis and on response to chemotherapy. Clin. Cancer Res. **7**: 1661–1668.
15. Wang, G. L., Jiang, B. H., Rue, E. A. and Semenza, G. L. (1995) Hypoxia-inducible factor 1 is a basic-helix-loop-helix-PAS heterodimer regulated by cellular O2 tension. Proc. Natl. Acad. Sci. U S A. **92**: 5510–5514.
16. Kallio, P. J., Pongratz, I., Gradin, K., McGuire, J. and Poellinger, L. (1997) Activation of hypoxia-inducible factor 1alpha: posttranscriptional regulation and conformational change by recruitment of the Arnt transcription factor. Proc. Natl. Acad. Sci. U S A. **94**: 5667–5672.
17. Jaakkola, P., Mole, D. R., Tian, Y. M., Wilson, M. I., Gielbert, J., Gaskell, S. J., Kriegsheim, A. v., Hebestreit, H. F., Mukherji, M., Schofield, C. J., Maxwell, P. H., Pugh, C. W. and Ratcliffe, P. J. (2001) Targeting of HIF-alpha to the von Hippel-Lindau ubiquitylation complex by O2-regulated prolyl hydroxylation. Science. **292**: 468–472.
18. Semenza, G. L. (2001) HIF-1, O(2), and the 3 PHDs: how animal cells signal hypoxia to the nucleus. Cell. **107**: 1–3.
19. Wang, G. L. and Semenza, G. L. (1993) General involvement of hypoxia-inducible factor 1 in transcriptional response to hypoxia. Proc. Natl. Acad. Sci. U S A. **90**: 4304–4308.
20. Norris, M. L. and Millhorn, D. E. (1995) Hypoxia-induced protein binding to O2-responsive sequences on the tyrosine hydroxylase gene. J. Biol. Chem. **270**: 23774–23779.
21. Shibata, T., Akiyama, N., Noda, M., Sasai, K. and Hiraoka, M. (1998) Enhancement of gene expression under hypoxic conditions using fragments of the human vascular endothelial growth factor and the erythropoietin genes. Int. J. Radiat. Oncol. Biol. Phys. **42**: 913–916.
22. Shibata, T., Giaccia, A. J. and Brown, J. M. (2000) Development of a hypoxia-responsive vector for tumor-specific gene therapy. Gene Ther. **7**: 493–498.
23. Aboagye, E. O., Lewis, A. D., Johnson, A., Workman, P., Tracy, M. and Huxham, I. M. (1995) The novel fluorinated 2-nitroimidazole hypoxia probe SR-4554: reductive metabolism and semiquantitative localisation in human ovarian cancer multicellular spheroids as measured by electron energy loss spectroscopic analysis. Br. J. Cancer. **72**: 312–318.
24. Seddon, B. M., Payne, G. S., Simmons, L., Ruddle, R., Grimshaw, R., Tan, S., Turner, A., Raynaud, F., Halbert, G., Leach, M. O., Judson, I. and Workman, P. (2003) A phase I study of SR-4554 via intravenous administration for noninvasive investigation of tumor hypoxia by magnetic resonance spectroscopy in patients with malignancy. Clin. Cancer Res. **9**: 5101–5112.
25. Koch, C. J and Evans, S. M. (2003) Non-invasive PET and SPECT imaging of tissue hypoxia using isotopically labeled 2-nitroimidazoles. Adv. Exp. Med. Biol. **510**: 285–292.
26. Durand, R. E. and Raleigh, J. A. (1998) Identification of nonproliferating but viable hypoxic tumor cells *in vivo*. Cancer Res. **58**: 3547–3550.
27. Nordsmark, M., Loncaster, J., Aquino-Parsons, C., Chou, S. C., Ladekarl, M., Havsteen, H., Lindegaard, J. C., Davidson, S. E., Varia, M., West, C., Hunter, R., Overgaard, J. and Raleigh, J. A. (2003) Measurements of hypoxia using pimonidazole and polarographic oxygen-sensitive electrodes in human cervix carcinomas. Radiother. Oncol. **67**: 35–44.
28. Semenza, G. L. (2003) Targeting HIF-1 for cancer therapy. Nat. Rev. Cancer. **3**: 721–32.
29. Laughner, E., Taghavi, P., Chiles, K., Mahon, P. C. and Semenza, G. L. (2001) HER2 (neu) signaling increases the rate of hypoxia-inducible factor 1alpha (HIF-1alpha) synthesis: novel mechanism for HIF-1-mediated vascular endothelial growth factor expression. Mol. Cell. Biol. **21**: 3995–4004.
30. Zhong, H., Chiles, K., Feldser, D., Laughner, E., Hanrahan, C., Georgescu, M. M., Simons, J. W. and Semenza, G. L. (2000) Modulation of hypoxia-inducible factor 1alpha expression by the epidermal growth factor/phosphatidylinositol 3-kinase/PTEN/AKT/FRAP pathway in human prostate cancer cells: implications for tumor angiogenesis and therapeutics. Cancer Res. **60**: 1541–1545.
31. Fukuda, R., Hirota, K., Fan, F., Jung, Y. D., Ellis, L. M. and Semenza, G. L. (2002) Insulin-like growth factor 1 induces hypoxia-inducible factor 1-mediated vascular endothelial growth factor expression, which is dependent on MAP kinase and phosphatidylinositol 3-kinase signaling in colon cancer cells. J. Biol. Chem. **277**: 38205–38211.
32. Maxwell, P. H., Wiesener, M. S., Chang, G. W., Clifford, S. C., Vaux, E. C., Cockman, M. E., Wykoff, C. C., Pugh, C. W., Maher, E. R. and Ratcliffe, P. J. (1999) The tumour suppressor protein VHL targets hypoxia-inducible factors for oxygen-dependent proteolysis. Nature. **399**: 271–275.